Engineering Structures 301 (2024) 117373

Contents lists available at ScienceDirect

Engineering Structures

journal homepage: www.elsevier.com/locate/engstruct

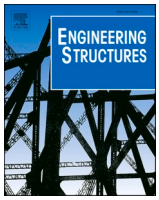

Virtual modelling aided safety assessment for ductile structures against high-velocity impact

Yuan Feng [a,b], Mehrisadat Makki Alamdari [a], Di Wu [c], Zhen Luo [d], Dong Ruan [e], Temitope Egbelakin [b], Xiaojun Chen [a], Wei Gao [a,*]

[a] Centre for Infrastructure Engineering and Safety (CIES), School of Civil and Environmental Engineering, The University of New South Wales, Sydney, NSW 2052, Australia
[b] School of Architecture and Built Environment, The University of Newcastle, Callaghan, Australia
[c] Centre for Built Infrastructure Research (CBIR), School of Civil and Environmental Engineering, University of Technology Sydney, Sydney, NSW 2007, Australia
[d] School of Mechanical and Mechatronic Engineering, University of Technology Sydney, Sydney, NSW 2007, Australia
[e] School of Engineering, Swinburne University of Technology, Hawthorn, VIC 3122, Australia

ARTICLE INFO

Keywords:
High-velocity impact
Ductile material
Virtual modelling
Machine learning
Safety assessment

ABSTRACT

This paper introduces a virtual modelling-aided computational analysis framework for assessing the safety of a ductile engineering object against high-velocity impact. By evaluating the data feedback continuously collected from the working site, the presented Virtual Modelling Aided Safety Assessment (VMASA) scheme is competent to effectively report the current safety level of the engineering object. The safety level (alternatively known as the reliability), of the impacted system can be quantified by using the first-passage theory. By considering various mercurial factors that are influencing the high-velocity impact for ductile materials, in this research, a new machine learning-aided virtual modelling technique as the clustering extended support vector regression (CXSVR), is implemented to evaluate the capacity of the engineering product against different conditions. Also, the John-Cook failure model is transformed into a random format to simulate the dynamic response of the engineering product against high-velocity impacts. A new T-spline kernel has also been developed within the CXSVR scheme. By using the VMASA, the inherent limit state function can be quantitatively certified by analysing the relationship between the system inputs and outputs. Both experimental and numerical investigations are implemented to demonstrate the accuracy, practicability, and efficiency of the proposed safety assessment framework.

1. Introduction

Structures made from metallic, or alloy materials are frequently facing the lurking effects of high dynamic loadings, such as the high-velocity impact of bird strikes, flying debris and burst stone [1–3], as shown in Fig. 1. The constant repair or patch for structural components bring huge capital costs, sometimes the entire structure needs to be replaced. Thus, this highlights the importance of safety assessment of structures against potential impact events, to prevent catastrophic consequences [4,5]. Furthermore, the nondeterministic parameters, for instance, the material properties, dynamic excitations, and dimensions of the structure have been inherently related to the entire system and could generate considerable fluctuations in the ultimate safety conditions [6,7]. The reliability analysis of structural systems is a significant solution to solve static safety problems and quantify the probability of failure. However, by incorporating the time-dependent random modelling process into the reliability framework, the overall dynamic safety assessment procedure would become extremely complicated.

In the past decades, many attempts have been made to investigate dynamic safety problems [8–10], which mainly use the first-passage theory to evaluate the probability of failure through numerical and analytical methods. The analytical solutions are normally acquired by two directions. One approach often used assumes of the Poisson process model and its modified versions [11]. In this method, the evaluation of reliability involves adopting the ratio of expected crossings and the extreme value distribution [12,13]. Nevertheless, this method is primarily applicable to linear systems excited by Gaussian white noises. Another approach involves assuming Markov diffusion processes [14].

* Corresponding author.
E-mail address: w.gao@unsw.edu.au (W. Gao).

https://doi.org/10.1016/j.engstruct.2023.117373
Received 21 May 2023; Received in revised form 13 December 2023; Accepted 15 December 2023
Available online 26 December 2023

(a) (b) (c)

Fig. 1. Structures: (a) automobile, (b) turbine engine, (c) stahlhelm under high-velocity impacts.

In this context, reliability is characterized by the conditional reliability function and the moments of the first-passage time. Although the second method offers increased accuracy, it necessitates solving partial differential equations. Due to the inherent difficulty in obtaining exact solutions for these equations, researchers often turn to approximate analytical solutions [15] and numerical techniques such as the finite difference method [16], finite element method [17], and similar approaches. However, the adoptions of these analytical and numerical methods are suitable in a limited range, which could be mainly useful in linear elastic problems for a single degree of freedom body, due to their inherent complexity in mathematic derivations and formulations [18]. That is, facing the high-velocity impact or other nonlinear problems, the time-dependent reliability function underpinned with the elastoplastic constitutive equation can be extremely difficult to acquire, let alone the continuous variations of material properties.

As another challenging issue, the capability of analysing structural safety during a time-dependent random modelling process is difficult to achieve. For most methodologies, reliability is focused on the ultimate response of structure within a period [19,20]. But for high-velocity impact problems, the structural deflection and impact energy is not proportionally increasing but varied along the time domain [21,22], which means the maximum dynamic responses would occur at any moment of the loading process. This highlights the importance of simulating and forecasting structural safety throughout the whole serving stage, particularly for sensitive structures under extreme working conditions [23]. By using the classical first-passage theory-based reliability analysis models, an overall approximation of the entire dynamic process can be obtained, which has been seen as critical for the modern dynamic systems. Furthermore, considering the randomness involved in the sampling-based dynamic safety assessment analysis, the impact responses of the concerned structure can be varied under different material properties, dynamic excitations, and dimensions of the structure, from which the integral result of the reliability cannot fully represent the safety condition of the structure. Consequently, a powerful safety forecast regime of structure is needed to observe real-life safety assessment problems.

Moreover, for the uncertainty involved dynamic structural analysis, the computational efficiency problem has always been an obstacle for various disciplines. In this research, the proposed framework is expected to predict structural potential response against continuously varying working information in a rapid manner. Then a quick and accurate safety forecast system for the structure can be achieved. Due to the elastoplastic constitutive equation of the ductile structure, the plastic deformation modelling under impact loadings is complex and time-consuming, which is not achievable through the integral type of analysis, i.e., first or second-order reliability method [24,25]. By using the sampling-based crude Monte Carlo simulation method [26], the probability of failure can be evaluated but a great quantity of repetitive deterministic finite element analysis is needed to calculate every possible response, which could result in tremendous computational efforts. Considering the practical needs, the computational efficiency of the modern reliability framework must be enhanced to a high dimensional level to surpass the analytical and numerical burdens.

There are clearly some essential requirements for modern engineering safety guidance: rapid simulating and adaptivity with varying inputs from surrounding observations. Models of conventional first-passage-based uncertainty quantification methods are impractical to fulfil all the standards. However, the decision-making ability by using the popular machine learning algorithm is a powerful alternative [27,28]. Various machine learning models have been widely adopted in different real-life engineering damage, nonlinear and reliability problems and have been validated effectively [29–31]. In this study, a new virtual modelling technique is introduced by enhancing the capability of machine learning algorithms with an efficient visualization module. The critical issues as mentioned can be addressed with new solutions.

First, the virtual modelling technique can analyse the inherent relationship with the varying inputs and structural impact responses at discretised time steps, in form of explicit functions. By using the well-known Johnson-Cook failure model [32,33], the random ductile damage governing equation under high-velocity impact can be determined by the sampling-basis of the machine learning algorithm, such that the structural response at an arbitrary moment can be estimated through the acquired functions. That is, the entire impact performance of the concerned structure can be monitored and controlled within a time-dependent loading process. By setting the safety threshold for the structure in advance, any predicted deflection or stress response exceeding the limit can be forecasted as an alarm state, which is known as the rapid simulating process. For this ability, accurate prediction is of vital importance to support. In addition, rapid simulation under various inputs from observations is another key feature of the proposed virtual modelling framework. Utilizing the obtained input-output functions, the estimated impact responses can be directly obtained, instead of running repetitive time-consuming finite element analysis. Then the predicted result can be implemented into the first passage theory to certify the limit state condition of the structure and complete a quick safety evaluation cycle. Actually, the specific failure criteria can be defined by different rules, and either the maximum displacement-based or residual velocity-based first-passage theory can be adopted. The proposed regime can integrate numerous historical data to train the model, then self-adapt with renewed information and quickly make a judgement on the current safety level of the engineering object.

In this paper, a virtual modelling-aided safety assessment (VMASA) scheme is proposed for ductile systems under high-velocity impact. A major objective is to establish efficient safety assessment that provides valid reports of the current safety level or reliability of the engineering object to the end-users, by rapidly evaluating data sources continuously collected from the working site. To support the functionalities, a new artificial intelligence technique as the clustering extended support vector regression, along with a newly developed T-spline kernel, has been incorporated into the Johnson-Cook ductile damage model against

random high-velocity impacts. Furthermore, the established VMASA framework in this paper has the prospective utility to involve different failure models and dynamic systems.

The paper is structured as follows. Section 2 introduces a brief review of the dynamic safety assessment of ductile impact damage, including the Johnson-Cook ductile damage model and the first-passage theory. Section 3 presents the nondeterministic structural dynamic safety analysis by using virtual modelling. Then the capability of the proposed VMASA framework is demonstrated through two practical examples in Section 4. Finally, some conclusions of the study have been drawn in Section 5.

2. The sampling-based dynamic safety assessment of ductile impact damage

2.1. Plastic deformation modelling under high-velocity impact

For ductile materials subjected to high-velocity impact, the relationship between the plastic stress and strain can be described through the popular Johnson-Cook model [34], which has been rigorously tested under large deformation and high strain rate conditions. Specifically, for an arbitrary status of structure with plastic deformation, the typical decomposition of the entire strain at a certain time step can be represented as

$$\boldsymbol{\varepsilon} = \boldsymbol{\varepsilon}_e + \boldsymbol{\varepsilon}_p \tag{1}$$

where $\boldsymbol{\varepsilon}_e$, $\boldsymbol{\varepsilon}_p$ are the linear elastic and plastic strains, respectively. Then a von Mises yielding function has been chosen to simulate the plastic stress flow, given as

$$\phi\left(\sigma, H\left(\varepsilon_p, T\right)\right) = \sqrt{3J_2/2} - H\left(\varepsilon_p, T\right) \tag{2}$$

where J_2 is the second deviatoric stress invariant, $H(\varepsilon_p, T)$ is the hardening matrix associated with plastic strain and temperature. And the hardening stress with the Johnson-Cook model can be represented as

$$\sigma = \left(\sigma_Y + H\bar{\varepsilon}_p\right)\left(1 + C\ln\dot{\bar{\varepsilon}}_p^*\right)\left(1 - T^{*m}\right) \tag{3}$$

where σ_Y denotes the yield stress; H denotes the straining hardening parameter; C is the material constant; $\dot{\bar{\varepsilon}}_p^* = \dot{\bar{\varepsilon}}_p/\dot{\varepsilon}_0$ denotes the dimensionless strain rate, $\dot{\varepsilon}_0$ is the reference strain rate; T^{*m} denotes the homologous melting temperature from the test [32]. In this study, regarding the experimental limitations, $\dot{\varepsilon}_0$ and T^{*m} are both taken as constants [35].

Thus, the associate flow rule can be transformed as

$$\varepsilon_p = \lambda\frac{\partial\phi\left(\sigma, H\left(\varepsilon_p, T\right)\right)}{\partial\sigma} \tag{4}$$

where λ is the plastic multiplier where the initiation of failure strain is generated. After plastic strain has been initialized, the damage evolution law of the fracture strain based on the Johnson-Cook failure criterion can be given as

$$\varepsilon_f = \left[D_1 + D_2\exp\left\{D_3\left(\frac{\sigma_m}{\sigma_{eq}}\right)\right\}\right]\left\{1 + D_4\ln\left(\dot{\bar{\varepsilon}}_p^*\right)\right\}\left(1 + D_5T^{*m}\right) \tag{5}$$

where D_1 to D_5 are material constants acquired from experiments; σ_m denotes the mean stress value; σ_{eq} denotes the equivalent stress.

With the incremental accumulation of plastic damage in the structural body, a damage parameter γ can be formulated to weaken the original stiffness as [36]:

$$\gamma = \sum\left(\frac{\Delta\varepsilon_p}{\varepsilon_f}\right) \tag{6}$$

where $\Delta\varepsilon_p$ is the incremental plastic strain. Consequently, considering the material strength loss during plastic deformation, the constitutive equation with the coupled elastic-plastic-damage relation on an individual element can be defined by

$$\boldsymbol{\sigma} = w(\gamma)\mathbf{D} : \boldsymbol{\varepsilon}_e = w(\gamma)\mathbf{D} : \left(1 - \boldsymbol{\varepsilon}_p\right) \tag{7}$$

with

$$w(\gamma) = 1 - \gamma \tag{8}$$

where $w(\gamma)$ is the weakening function with damage parameter γ; $\mathbf{D}$ is the normal linear stiffness matrix of the structure.

Subsequently, considering the contributions from all elements and different time steps discretised from the dynamic loading process, by using the principle of virtual work, the global governing equation for the incremental plastic deformation modelling subjected to impact loadings can be represented as

$$\mathbf{K}_{ep}^{w}\cdot\Delta\mathbf{U}(t) = \left(1 - \boldsymbol{\gamma}\right)\mathbf{K}_{ep}\cdot\Delta\mathbf{U}(t) = \Delta\mathbf{F}(t) \tag{9}$$

where $\mathbf{K}_{ep}^{w}$ is the weakened global elastoplastic stiffness matrix with damage vector $\boldsymbol{\gamma}$; $\Delta\mathbf{U}(t)$ is the incremental displacement vector which is time-dependent; $\Delta\mathbf{F}(t)$ is the time-dependent incremental external loading vector. Therefore, the entire process of the structure from undamaged state until fully penetration collapse considering plastic behaviour can be obtained.

2.2. Nondeterministic impact response of structure

In real-life engineering applications, the material properties can be varied under different scenarios, for instance, the Young's modulus E, Poisson's ratio υ, yield stress σ_Y, hardening parameter H and material density ρ etc. In this section, the randomness of each factor is implemented by sampling different distribution types and information to the deterministic values through quasi-Monte Carlo Sobol's sequence method [37], which can be represented by $\boldsymbol{\xi} = \{E(\zeta), \upsilon(\zeta), \sigma_Y(\zeta), H(\zeta), \rho(\zeta).\}$ [38]. From which, $\boldsymbol{\xi}$ is a random vector collecting different variations of system properties in the probability space, and ζ represents one possible realization of the random variable set. By doing so, the random vector can then be adopted into the deterministic plastic impact damage deformation model to obtain the quantified nondeterministic impact responses of the concerned structure.

As mentioned, the nondeterministic hardening plastic stress by using the Johnson-Cook model can be reformulated as

$$\sigma(\zeta) = \left\{\sigma_Y(\zeta) + H(\zeta)\bar{\varepsilon}_p\right\}\left(1 + C\ln\dot{\bar{\varepsilon}}_p^*\right)\left(1 - T^{*m}\right) \tag{10}$$

where $\sigma(\zeta)$ is the nondeterministic expression of plastic stress. For individual elements, the random constitutive equation can be expressed as

$$\boldsymbol{\sigma}(\zeta) = \left(1 - \gamma\right)\mathbf{D}(\zeta) : \left(1 - \boldsymbol{\varepsilon}_p(\zeta)\right) \tag{11}$$

By considering various random vectors, the global governing equation for dynamic impact responses of ductile structure can be changed to

$$\mathbf{K}_{ep}^{w}(\boldsymbol{\xi})\cdot\Delta\mathbf{U}\left(\boldsymbol{\xi}, t\right) = \left(1 - \boldsymbol{\gamma}\right)\mathbf{K}_{ep}(\boldsymbol{\xi})\cdot\Delta\mathbf{U}\left(\boldsymbol{\xi}, t\right) = \Delta\mathbf{F}\left(\boldsymbol{\xi}, t\right) \tag{12}$$

where $\mathbf{K}_{ep}^{w}(\boldsymbol{\xi})$, $\Delta\mathbf{U}(\boldsymbol{\xi}, t)$ and $\Delta\mathbf{F}(\boldsymbol{\xi}, t)$ are the weakened global elastoplastic stiffness matrix, time-dependent incremental displacement, and external loading vector in nondeterministic formats.

It should be stated although the governing equation has been acquired, the explicit or analytical solution of $\mathbf{U}(\boldsymbol{\xi}, t)$ are only available to very simplified cases rather than real-life engineering applications with complex geometries or degrees of freedom [39]. Thus, the detailed quantification of the distributed probability density function (PDF) of $\mathbf{U}(\boldsymbol{\xi}, t)$ is computationally infeasible. In the past decades, considering various numerical approaches to approximate the statistical moments

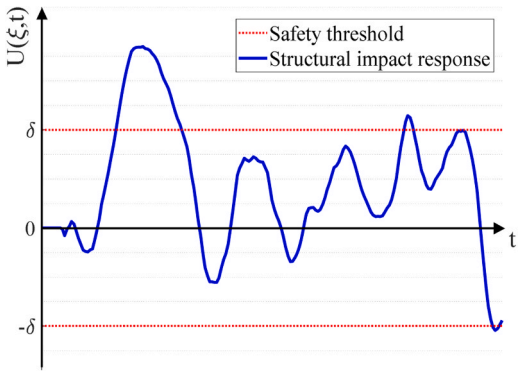

Fig. 2. The safety threshold in first-passage theory.

and reliability profiles of nondeterministic impact response of structures, the crude Monte Carlo simulation (MCS) approach has been considered as an applicable method and has been widely used in different circumstances [40].

2.3. First-passage failure principle

The safety condition for the structure can generally be assessed through evaluating the failure probability based on structural responses, for instance the maximum displacement, stress or stain within the body undergoes dynamic loadings. Typically, the structure is determined as failed if the structural response reaches or exceeds the pre-set safety threshold at the first time, which has been known as the first-passage failure principle. From analytical discipline, the probability of failure can be calculated by

$$P_f = \Pr\left\{g(\boldsymbol{\xi}) \le 0\right\} = \int_{g(\boldsymbol{\xi})\le 0} f_{\boldsymbol{\xi}}^{\mathrm{PDF}}(\boldsymbol{\xi})d\boldsymbol{\xi} = \int_{\Re^n} [[g(\boldsymbol{\xi}) \le 0] f_{\boldsymbol{\xi}}^{\mathrm{PDF}}(\boldsymbol{\xi})d\boldsymbol{\xi} \tag{13}$$

where $\Pr\{\cdot\}$ is the probability space; $[[\cdot]$ denotes an indicator function that will equal to 1 when $[\cdot]$ is 'true', otherwise 0 when $[\cdot]$ is 'false'; $f_{\boldsymbol{\xi}}^{\mathrm{PDF}}(\boldsymbol{\xi})$ is the PDF for $\boldsymbol{\xi}$; $g(\boldsymbol{\xi})$ is the limit state function defining structural failure when $g(\boldsymbol{\xi}) \le 0$.

It should be noticed that, for structural dynamics, the responses are varied along the time domain, so as the corresponding limit state function. Thus, the time-dependent probability of failure in a time interval $[0, T]$ can be reformulated as

$$P_f = \Pr\{\exists t \in [0,T], g(\boldsymbol{\xi}, t) \le 0\} \tag{14}$$

otherwise, in the format of exceeding safety threshold δ as shown in Fig. 2, with

$$P_f = \Pr\{\exists t \in [0,T],\ \max \_\mathbf{U}(\boldsymbol{\xi}, t) \ge |\delta|\} \tag{15}$$

where $g(\boldsymbol{\xi}, t) = |\delta| - \max \_\mathbf{U}(\boldsymbol{\xi}, t)$ can be transformed from each format. Therefore, the robust way to accurately and efficiently obtain P_f is still a challenging task in practical impact reliability analysis. Among the established mathematical models to get the probability of failure, for instance the Markov models, the detailed expression can be defined by

$$\begin{cases} v^+(t) = \lim\limits_{\Delta t\to 0} \dfrac{\Pr\{g(\boldsymbol{\xi}, t) > 0 \cap g(\boldsymbol{\xi}, t+\Delta t) < 0\}}{\Delta t} \\ P_f = 1 - \exp\left[-\displaystyle\int_0^T \frac{v^+(t)}{1 - P_{f,ins}(t)} dt\right] \end{cases} \tag{16}$$

where $v^+(t)$ is the out-crossing rate, $p_{f,ins}(t) = \Pr\{g(\mathbf{x}, t) \le 0\}$ denotes the instantaneous probability of failure at time t. It can be observed from the Markov model that the formulation requires large calculations of out-crossing rates and a complex integral process for the entire time domain [12], which is extremely complex and time-consuming in the real-life engineering applications, especially against the high-dimensional nondeterministic features. Thus, in the study, the crude MCS approach is employed to evaluate the probability of failure through an effective sampling approach [41], by generating large number of samples n for the input vector $\boldsymbol{\xi}_i (i = 1, 2, ., n)$, the P_f can be alternatively expressed as

$$P_f \approx \widehat{P}_f = \frac{1}{n}\sum_{i=1}^{n} [[g(\boldsymbol{\xi}_i \le 0)] = \frac{n_f}{n} \tag{17}$$

where n_f is the total number of samples resulting in the failure of structure.

Based on Eq. (17), an alternative solution is provided for acquiring the probability of failure in both structural deformation and strength fields. However, as seen from the expression of P_f, the determination of the safety or reliability of structure still requires a complete realization of all generated samples in the whole dynamic loading process [42,43]. That is, a large number of computational efforts are used to repeatedly calculate the physical finite element analysis for complicated structures and consistently evaluate the limit state function [44]. Moreover, this computational barrier will be raised to another high-dimensional untouchable level, if the system properties are continuously changing under dynamic circumstances. Facing with this condition, a machine learning aided virtual modelling reliability analysis is a powerful alternative, which could efficiently analyse the correlation between the random inputs and system response outputs.

3. Structural dynamic safety analysis by using virtual modelling

In this section, the new virtual-modelling safety assessment technique (VMASA) aided by a newly developed machine learning algorithm is proposed to solve the structural sampling-based dynamic safety assessment problems with much less computational efforts required in comparison with the classical MCS approach. The new artificial intelligence technique as the clustering extended support vector regression (CXSVR), along with a newly developed T-spline kernel to reinforce the performance of virtual model are introduced. Then, a detailed introduction of the construction of structural dynamic safety analysis by using the proposed model will be presented.

3.1. Kernelized CXSVR

Stimulating by conventional support vector machine employed in a variety of engineering fields [45], different machine learning algorithms based on various theories have been popular among practical applications [46–48]. In this study, aiming at complex physical process and high-efficiency handling capability, a freshly developed machine learning algorithm, namely the clustering extended support vector regression (CXSVR) has been established. Parallel training clusters and high-dimensional feature transform have been brought together into the algorithm [49,50], so complicated engineering applications with changing working scenarios could be quantified accurately.

Assume a group of random vectors $\boldsymbol{\xi}_j (j = 1, 2, ., m)$ in a relative disordered sequence, the kernelized mapping process within the technique can raise the random vector into a high-dimensional structured pattern, which can be represented as

$$\boldsymbol{\xi} = [\xi_1, \xi_2, ., \xi_j]^T \Rightarrow \widehat{\mathbf{k}}(\boldsymbol{\xi}_j) = \begin{bmatrix} \boldsymbol{\Theta}(\boldsymbol{\xi}_1)^T \boldsymbol{\Theta}(\boldsymbol{\xi}_j) \\ \boldsymbol{\Theta}(\boldsymbol{\xi}_2)^T \boldsymbol{\Theta}(\boldsymbol{\xi}_j) \\ \vdots \\ \boldsymbol{\Theta}(\boldsymbol{\xi}_m)^T \boldsymbol{\Theta}(\boldsymbol{\xi}_j) \end{bmatrix} = \begin{bmatrix} k(\boldsymbol{\xi}_1, \boldsymbol{\xi}_j) \\ k(\boldsymbol{\xi}_2, \boldsymbol{\xi}_j) \\ \vdots \\ k(\boldsymbol{\xi}_m, \boldsymbol{\xi}_j) \end{bmatrix}, j = 1, 2, ., m. \tag{18}$$

where $\boldsymbol{\Theta}(\boldsymbol{\xi}_j)$ is the implicit kernel mapping function; $\widehat{\mathbf{k}}(\boldsymbol{\xi}_j)$ is the jth kernelized feature vector.

In general, the optimization process of the kernelized clustering

Table 1
The mathematical measures.

Evaluation measures	Formulations
R-squared (R^2)	$R^2 = 1 - \frac{\sum_{i=1}^{\xi_{train}} (\widehat{y}_i - y_i)^2}{\sum_{i=1}^{\xi_{train}} (\mu_{yi} - y_i)^2}$
Root mean square error (RMSE)	$\mathrm{RMSE} = \sqrt{\frac{1}{\xi_{train}} \sum_{i=1}^{\xi_{train}} (\widehat{y}_i - y_i)^2}$
Relative error (RE)	$\mathrm{RE} = \frac{y_i - \widehat{y}_i}{y_i} \times 100\%$

*y_i, $\widehat{y}_i$ and $\mu_{\widehat{y}i}$ denote true, estimated and mean values of the responses at the ith sampling point.

extended support vector regression can be expressed as

$$\min_{\mathbf{p}_k, \mathbf{q}_k, \chi, \vartheta, \widehat{\vartheta}} : \frac{\lambda_1}{2}\left(\|\mathbf{p}_k\|_2^2 + \|\mathbf{q}_k\|_2^2\right) + \lambda_2 \mathbf{e}_m^T\left(\mathbf{p}_k + \mathbf{q}_k\right) + \frac{S}{2}\left(\vartheta^T\vartheta + \widehat{\vartheta}^T\widehat{\vartheta}\right) \tag{19}$$

$$\begin{cases} \mathbf{k}\left(\mathbf{p}_k - \mathbf{q}_k\right) - \chi\mathbf{e}_m^T - \mathbf{y}_{res} \le \varepsilon\mathbf{e}_m^T + \vartheta \\ \mathbf{y}_{res} - \left(\mathbf{k}\left(\mathbf{p}_k - \mathbf{q}_k\right) - \chi\mathbf{e}_m^T\right) \le \varepsilon\mathbf{e}_m^T + \widehat{\vartheta} \\ \mathbf{p}_k, \mathbf{q}_k, \vartheta, \widehat{\vartheta} \ge \mathbf{0}_m \end{cases} \tag{20}$$

where $\mathbf{y}_{res}$ is the structural response vector corresponding to $\xi_j (j = 1, 2, ., m)$; $\mathbf{p}_k, \mathbf{q}_k$ are positive coefficients; λ_1, λ_2 are tunning coefficients for feature selections; $\vartheta, \widehat{\vartheta}$ denote the slack parameter within a quadratic loss equation; χ is the bias coefficient; ε is the tolerable deviation be-

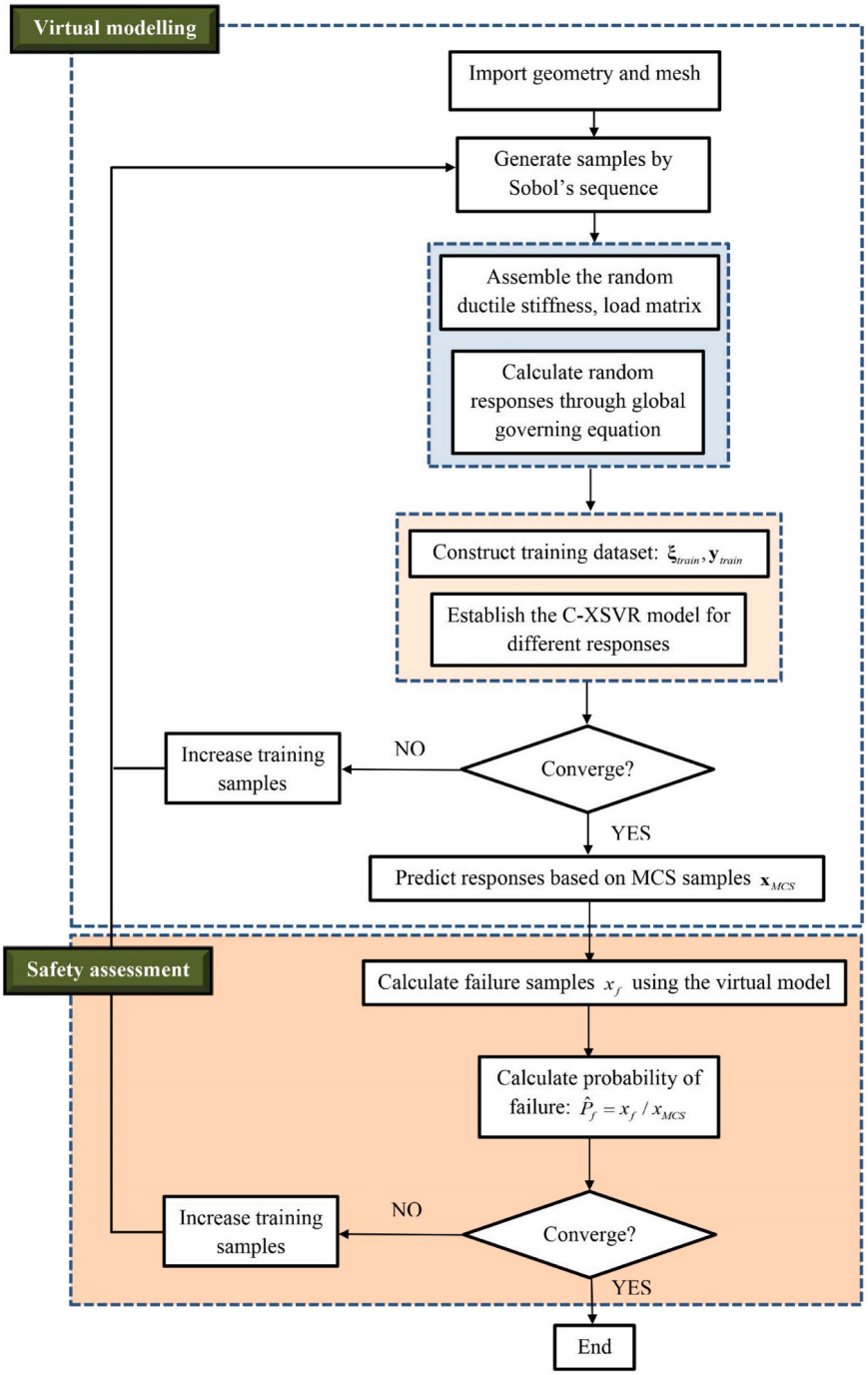

Fig. 3. Flowchart for structural dynamic safety analysis by using VMASA.

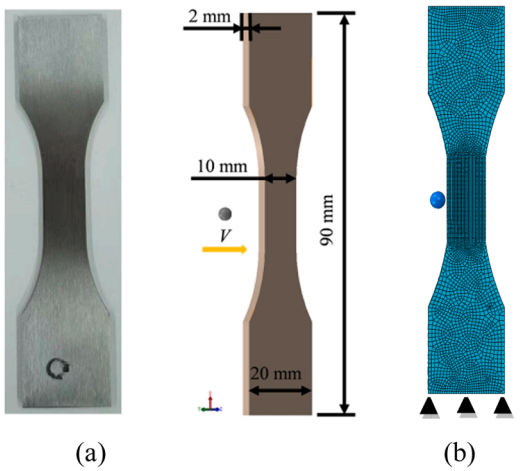

Fig. 4. Experimental case: (a) Dog-bone flat specimen [58], (b) FE mesh plot.

Table 2
Distribution inputs for the dog-bone flat specimen.

Varying Inputs	Distribution type	Mean	Standard deviation	Interval
E (GPa)	Lognormal[47]	122.6	6.1	-
υ	Beta	0.3	0.010	-
σ_Y (MPa)	Normal[28]	954.7	47.7	-
τ(mm)	Uniform[58]	–		[0,1]

tween the estimated and actual result. For the sake of simplicity, Eq. (19) can be modified as the following optimization function as [51]:

$$\min_{\mathbf{u}_k} : \frac{1}{2}\mathbf{u}_k^T\mathbf{Q}_k\mathbf{u}_k - \mathbf{m}_k^T\mathbf{u}_k \tag{21}$$

where $\mathbf{u}_k \in \Re^{4m}$ is the concerned solution of the optimization problem; $\mathbf{Q}_k \in \Re^{4m\times 4m}$ and $\mathbf{m}_k \in \Re^{4m}$ are explained with full details in Appendix A, due to page limitations.

Subsequently, by solving the above optimization problem with the acquired global optimal result $\mathbf{u}_k^*$, the explicit expression of the kernelized CXSVR function can be represented as

$$\widehat{f}(\boldsymbol{\xi}) = (\mathbf{p}_k - \mathbf{q}_k)^T\widehat{\mathbf{k}}(\boldsymbol{\xi}) - \mathbf{e}_k^T\mathbf{u}_k^* \tag{22}$$

It should be noticed that the ultimate performance of the regression function still depends on the kernel function $\widehat{\mathbf{k}}(\boldsymbol{\xi})$ selected, which will be introduced in the following section.

3.2. A new T-spline polynomial kernel function

For regression problems, especially nonlinear complex applications, the ultimate behaviour of the surrogate model relies on the kernel chosen [52]. The spline kernels have been very popular in interpolation and function estimation, for instance the well-known B-spline kernel or other basic spline [53,54]. The spline kernels are competent to effectively handle the local supports used for function approximation, and polynomial basis of the kernel receives increasingly interests from a variety of researchers.

In recent years, T-spline functions have been widely adopted for feature quantification and function approximation [55], due to its flexibility with multi-dimensional polynomial level and excellent refinement of complicated parameterization especially in isogeometric analysis. Stimulating by these features, we constructed a new T-spline kernel function for the proposed kernelized CXSVR. By defining on the selection region of $[-1,1]$, the T-spline kernel function $\mathbf{T}_{spline}(\boldsymbol{\xi}_i,\boldsymbol{\xi}_j)$ is expressed recursively as

$$\mathbf{T}_{spline}\left(\boldsymbol{\xi}_i,\boldsymbol{\xi}_j\right) = \frac{P_i w_i B_{2n+1}\left(\boldsymbol{\xi}_i - \boldsymbol{\xi}_j\right)}{\sum_{j=1}^{m} w_j B_{2n+1}\left(\boldsymbol{\xi}_i - \boldsymbol{\xi}_j\right)} \tag{23}$$

$$B_n(\boldsymbol{\xi}_i) = \sum_{r=0}^{i+1}\frac{(-1)^r}{i!}\frac{(i+1)!}{r!(i+1-r)!}\left(\boldsymbol{\xi}_i + \frac{i+1}{2} - r\right)_+^i \tag{24}$$

where $(\boldsymbol{\xi}_i)_+ = \max(0,\boldsymbol{\xi}_i)$; w_i denotes a set of positive weights; P_i denotes the spline coefficient; $B_n(\boldsymbol{\xi}_i)$ is a B-spline kernel; n denotes the degree of polynomial function.

It can be observed the range and shape of the polynomial kernel depends on the hyperparameter order n. Different interpolation and estimation accuracy could be resulted with different orders. Consequently, to effectively fulfill the purpose of auto-learning and auto-training skills of the T-spline polynomial kernel, the well-known Bayesian optimization method has been integrated within the proposed algorithm for better training purposes [56,57].

3.3. Virtual modelling aided safety assessment (VMASA) framework

In this research, a newly developed VMASA model is introduced to help predict the structural responses via sampling-based approach. Since the governing equation will be solved based on each data from the input vector $\boldsymbol{\xi}_i(i = 1,2,.,n)$, limit number of deterministic impact analyses are calculated at the sampling points. Within each realization, the deterministic dynamic response is discretized into a series of time steps. For each time step, the relationship between the input variables and structural outputs is approximated by the VMASA approach, which is an explicit formulation. After the regression formulation is acquired, the

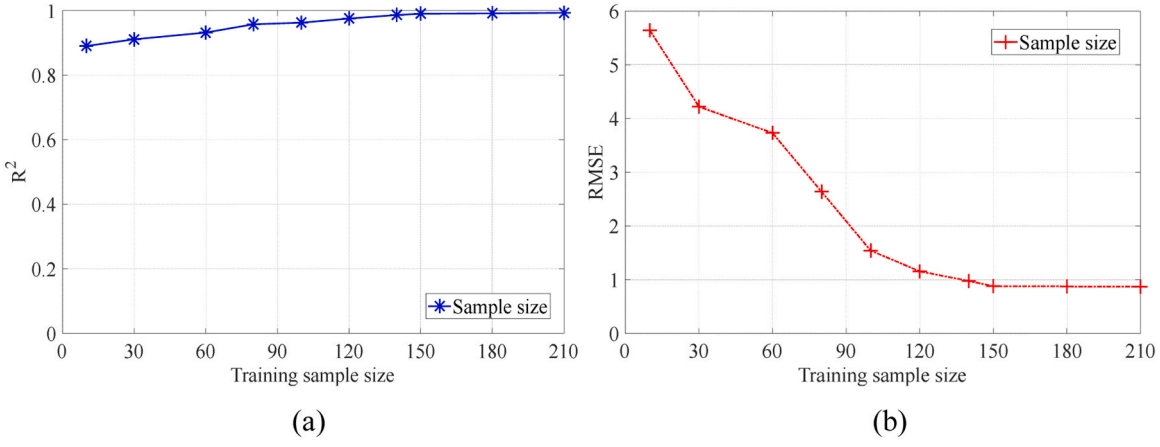

Fig. 5. The estimated (a) R^2 and (b) *RMSE* of impact energy with different sample sizes.

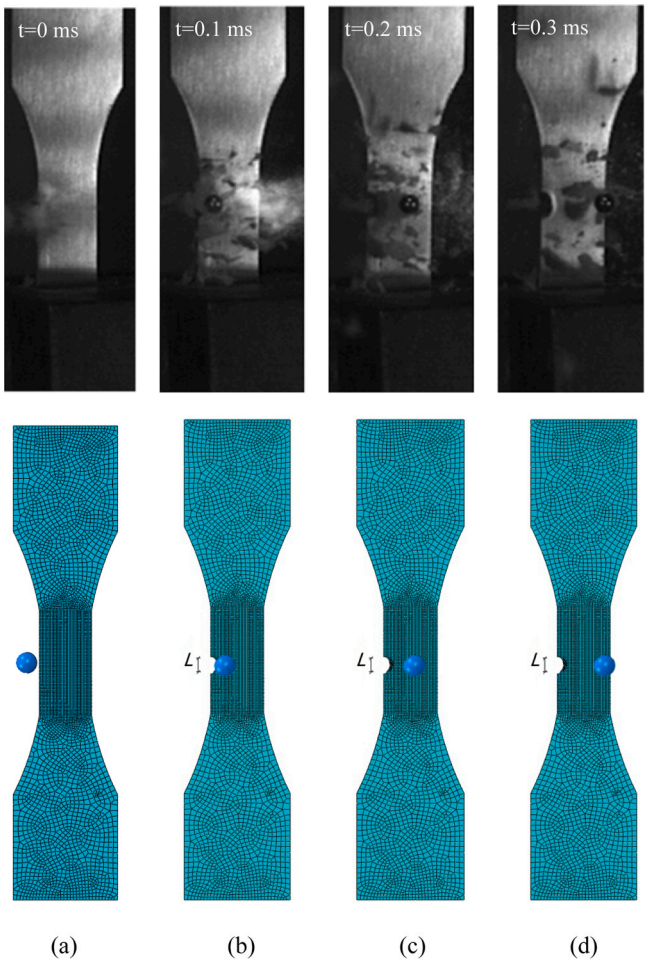

Fig. 6. Comparison of the impact process between the experimental test and VMASA predicted simulation at (a) $t = 0$ ms, (a) $t = 0.1$ ms, (a) $t = 0.2$ ms and (a) $t = 0.3$ ms.

Table 3
Results of experimental and predicted notch sizes L with different impact positions.

Impact offset position (mm)	Experimental test L (mm)	VMASA predict L (mm)
0	4.25	4.02
0.25	4.47	4.16
0.5	4.36	4.45
0.75	4.02	3.90
1	3.83	3.95

potential structural response at each time step can be directly predicted without the need of re-running the finite element analysis. Furthermore, with the implementation of clustering nodes, multiple time steps can be predicted simultaneously to construct the full loading process of dynamic event. For the structural dynamic safety analysis, the limit state function has been evaluated by the VMASA technique instead of the repetitive finite element analysis. Subsequently, the probability of failure of structure can be approximated through the virtual modelling based MCS sampling strategy. In general, the design of experiment (DoE) based principle is first adopted to make convergence study of the virtual model by using different levels of training samples through quasi-Monte Carlo simulation method with Sobol's sequence, which can guarantee to make reliable prediction compared with the MCS-derived results. This process is achieved through mathematic measures as listed in Table 1, as to draw convergence curve of prediction accuracy under various training samples.

For the dynamic safety analysis in this study, a safety threshold $|\delta|$ is taken as the barrier for the first-passage theory to record the failure conditions of structure. The detailed procedure of the dynamic safety analysis by using VMASA model can be summarized as

1. Input the structural geometry, mesh, system properties and loading conditions to the dynamic safety analysis framework.
2. Generate different DoE levels of training samples $\boldsymbol{\xi}_{train}$ by using the quasi-MCS Sobol's sequence and calculate the structural responses $\mathbf{y}_{train}$ through deterministic analysis.
3. If there are experimental results, use the experimental results as reference, otherwise, generate a large number of MCS samples $\mathbf{x}_{MCS}$ ($10^3 - 10^5$) with repetitive finite element results as reference. Then, compare the prediction results of different DoEs with reference through measures in Table 1, and certify the most converged training sample size.
4. Train the CXSVR models at different nodal points through the steps in Section 3.1 and establish the VMASA framework. The limit state function of the concerned response $\widehat{g}(\boldsymbol{\xi})$ can be approximately estimated through the obtained VMASA model.
5. Predict all the dynamic responses based on $\mathbf{x}_{MCS}$ and implement into the limit state function $\widehat{g}(\boldsymbol{\xi})$. Based on the failure criterion of $\widehat{g}(\boldsymbol{\xi}) \leq 0$, select all failure samples x_f.
6. The probability of failure for the response can be calculated through $\widehat{P}_f = x_f / x_{MCS}$.
7. Verify the estimated $\widehat{P}_f$ with the MCS-derived P_f. If the varying inputs are updated with new information, return to Step 5 and re-evaluate the probability of failure.

To provide a more distinct understanding, the flowchart of the dynamic safety analysis by using virtual modelling technique is shown in Fig. 3.

4. Numerical investigation

To illustrate the accuracy, efficiency and practicability of the sampling-based dynamic safety assessment for structure under high-velocity impact, one experimental validation and two practical engineering applications are investigated in this section. Considering varying inputs for the system parameters, the validation parameters in Table 1 have been used to verify the accuracy between predicted and reference results. The results are all completed on the workstation of Intel(R) Xeon(R) Gold 5215 CPU @ 2.5 GHz 10 cores with 192 GB RAM.

4.1. Experimental dog-bone flat specimen

In the first experimental validation case, the dog-bone flat specimen against high-velocity impact test is considered and compared with the experimental observations from Zhang et al. [58]. The dog-bone flat specimen is made of titanium alloy with dimensions of 90 mm × 20 mm× 2 mm and fixed at the bottom surface as shown in Fig. 4. The steel spherical projectile ($E = 220$ GPa, $\mu = 0.3$) with a diameter of 4 mm was accelerated by an air gun system at a speed of 350 m/s was conducted to impact normally to the edge of the flat specimen. In order to effectively verify the numerical simulated result, the FE model was established using Abaqus to simulate the high velocity test and the hexahedral elements (C3D8) with a total number of 18,392 were used to mesh the structure as shown in Fig. 4(b).

To construct the proposed VMASA surrogate model, the uncertainty information of Young's modulus E, Poisson's ratio υ, yield strength σ_Y and impact position τ (from the midline of specimen thickness to the edge) are considered for the flat specimen to establish a sufficient training dataset. The MCS simulation with 1000 cycles is used as reference. The detailed uncertainty information is listed in Table 2, with

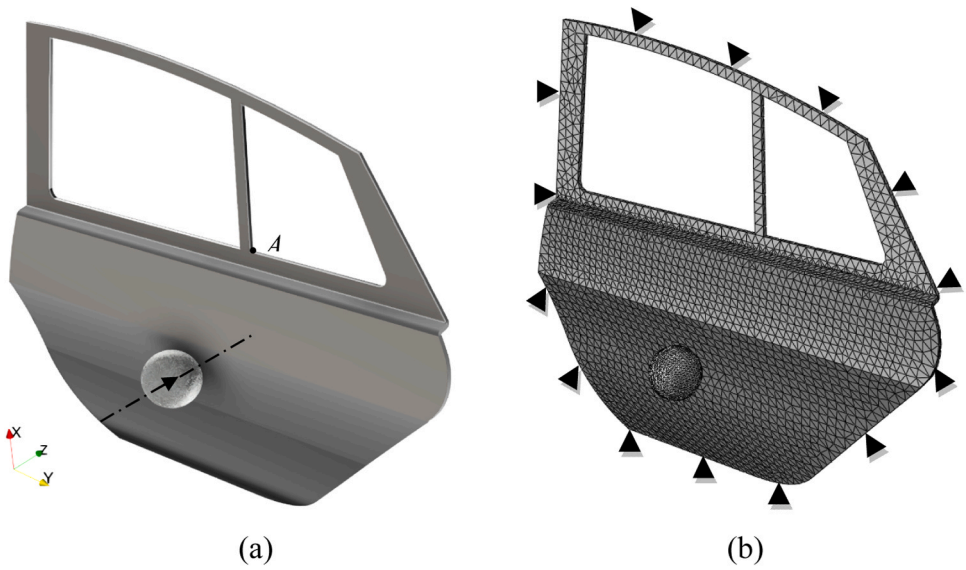

Fig. 7. Numerical example 2: (a) Car door geometry, (b) mesh plot and boundary conditions.

Table 4
Distribution inputs for the car door.

Varying Inputs	Distribution type	Mean	Standard deviation	Interval
E (MPa)	Normal[28]	2.1E5	11.2	-
υ	Beta	0.32	0.011	-
ρ (kg/m^3)	Uniform	–		[7515,8145]
σ_Y (MPa)	Lognormal[47]	700	35.3	-
H	Uniform	–		[1E3, 2E3]
v (m/s)	Weibull	60	3.10	-

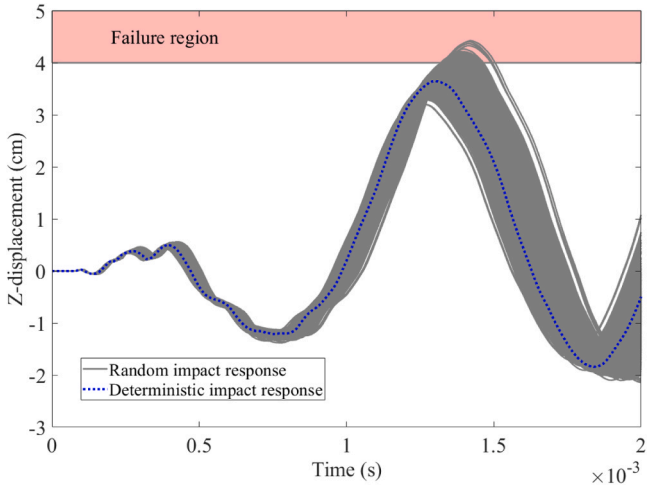

Fig. 8. Random impact responses and failure region at point A of the car door.

the random vector of $\boldsymbol{\xi} = \{E(\zeta), \upsilon(\zeta), \sigma_Y(\zeta), \tau(\zeta)\}$.

By observing the impact energy released within the dynamic process, the convergence study of the statistical measures of R^2 and RMSE through the proposed model with various sample sizes are demonstrated in Fig. 5. From Fig. 5, it is clear that with the increment of training sample size, the R^2 of trained impact energy rises from 0.891 to 0.993 at the sample size of 150, whilst the relevant RMSE decreases from 5.642 to 0.872. Thus, the training sample size of the VMASA model is determined as 150 for the flat specimen.

For the construction of the VMASA surrogate model, a total of 18,392 clusters were parallel trained to predict high impact energy, deflection, and stress within each FE element. As captured from the experimental test [58], a group of high-speed snapshots of projectile at the impact velocity of 350 m/s impacting on the flat specimen are shown in Fig. 6, in comparison with the VMASA numerical simulation results. As illustrated in Fig. 6, the edge of the specimen was penetrated through the dynamic impact process and a part of specimen was peeled off from both approaches. Therefore, the accuracy of the numerical simulation based VMASA model has been fully demonstrated through the experimental test results.

Moreover, a correlation on the damaged notch sizes L between the experimental and numerical results could also be investigated. When the impact position of projectile changes, the notch sizes would vary. The possible notch sizes can be directly predicted through the trained VMASA model. In Table 3, a series of different impact positions, as well as the corresponding experimental and predicted notch sizes are listed. From the table, the VMASA surrogate model predicted results exhibited similar notch sizes with the experimental results, and the accuracy of proposed approach could be acceptable considering the problem complexity.

4.2. Car door

For the second numerical case, a practical car door is impacted by a flying stone, with the impact velocity around 60 m/s. The car door is made of steel material and a strain hardening effect has been considered for the car door. The dimensions of the car door are simplified to 1.6 m × 1.2 m× 0.02 m and the diameter of the impactor is 0.25 m. The geometry of door and impactor are shown in Fig. 7(a), by using the tetrahedron element, a converged mesh of geometry is shown. For the boundary conditions of the car door application, the nodes on the external edges of the car door are fixed in all directions which have been highlighted in Fig. 7(b) through black triangular symbols and the z-direction impact loading was applied at the central location of the door surface.

For the car door application, in order to keep the passengers' safe, the engineering failure criteria should be more focused on the maximum deflection of car door under dynamic loadings. Thus, for this case, a maximum displacement based first-passage theory should be adopted. For instance, the maximum z direction displacement at point A on car B-pillar is selected as the observation response and the safety threshold at point A is set to be $|\delta| = 4$cm[59–61]. The maximum displacement-based

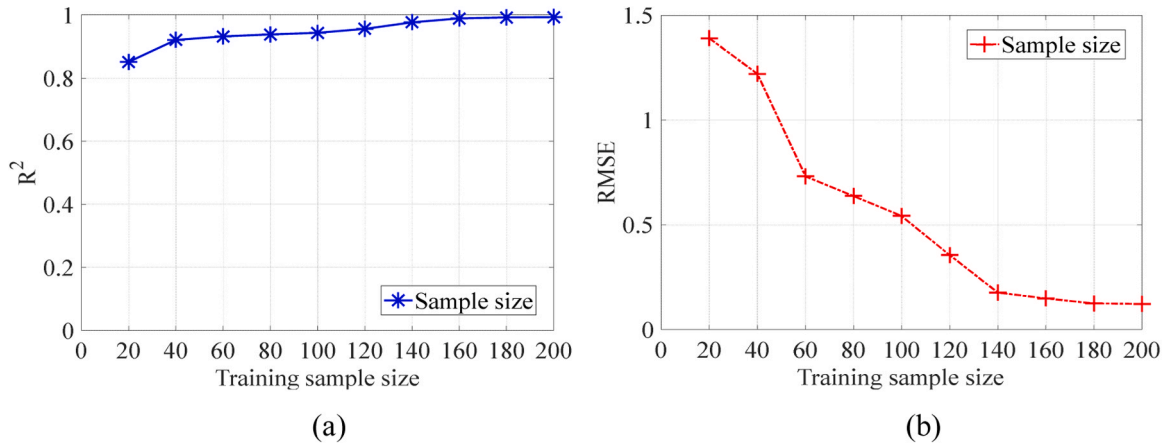

Fig. 9. The estimated (a) R^2 and (b) *RMSE* of Z-displacement with different training sample size.

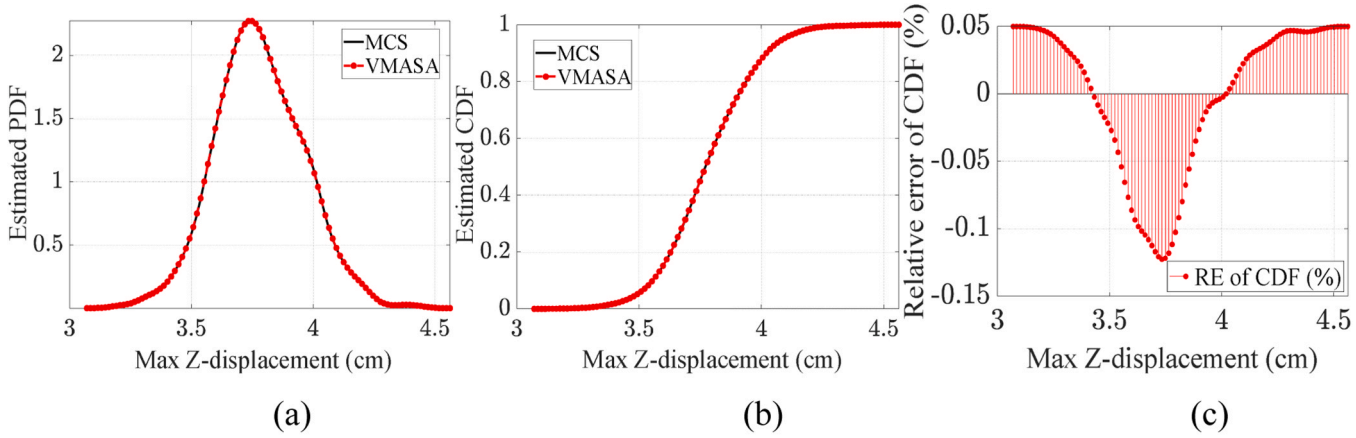

Fig. 10. (a) The estimated PDFs; (b) CDFs; (c) *RE* of CDFs of maximum Z-displacement.

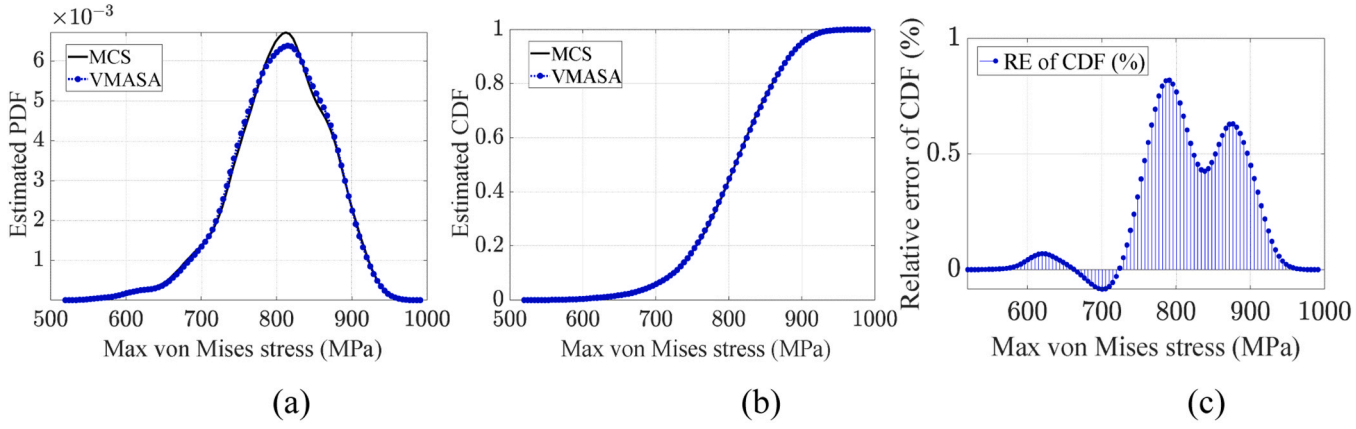

Fig. 11. (a) The estimated PDFs; (b) CDFs; (c) *RE* of CDFs of maximum von Mises stress.

Table 5
The estimated moments of max Z-displacement and von Mises (vM) stress.

Moments	Methods	Max Z-disp (cm)	*RE* (%)	Max vM stress (MPa)	*RE* (%)	Computational cost (h)
Mean	VMASA	3.781	0.0264	804.749	2.36E-3	34.1
	MCS	3.780	–	804.730	–	167.9
Std	VMASA	0.179	1.117	61.197	-3.27E-3	34.1
	MCS	0.177	–	61.199	–	167.9

Table 6
The probability of failure of max Z-displacement at point A exceeds $|\delta|$.

Methods	$\widehat{p}_f$ (N_{train}=50)	RE_{p_f} (%)	$\widehat{p}_f$ (N_{train}=100)	RE_{p_f} (%)	$\widehat{p}_f$ (N_{train}=200)	RE_{p_f} (%)
VMASA	0.075	-38.017	0.099	-18.182	0.122	0.826
MCS	$p_f = 0.121$					

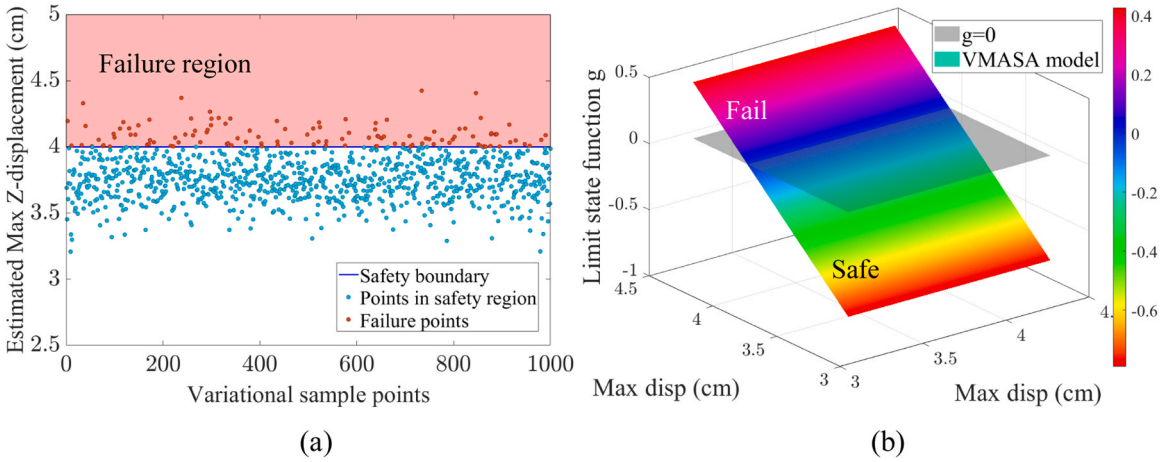

Fig. 12. (a) The estimated max Z-displacement and (b) limit state function at different input samples through the VMASA model.

Table 7
Arbitrary three groups of new input samples.

Varying Inputs	Sample I	Sample II	Sample III
E (MPa)	1.943E5	2.215E5	1.761E5
υ	0.3042	0.2893	0.3010
ρ (kg/m^3)	7652	7864	7594
σ_Y (MPa)	712.3	725.7	685.4
H	1323	1266	1851
v (m/s)	63.2	60.1	62.4

Table 8
The predicted safety status of car door with three arbitrary new samples.

Samples	Methods	Max Z-disp (cm)	RE (%)	Safety status	Computational cost (min)
I	VMASA	4.056	0.173	Fail, g= 0.056	0.083
	Numerical	4.049	–	Fail, g= 0.049	10.5
II	VMASA	3.561	0.112	Safe, g= −0.439	0.083
	Numerical	3.557	–	Safe, g= −0.443	10.5
III	VMASA	4.426	0.113	Fail, g= 0.426	0.083
	Numerical	4.421	–	Fail, g= 0.421	10.5

limit state function in this example is represented as

$$g(\boldsymbol{\xi}, t) = \max\_\mathbf{U}(\boldsymbol{\xi}, t) - |\delta| = \max\_\mathbf{U}(\boldsymbol{\xi}, t) - 4 \tag{25}$$

where the limit state function $g < 0$, the structure is safe, otherwise failed.

For the varying input samples, the random vector $\boldsymbol{\xi} = \{E(\zeta), \upsilon(\zeta), \sigma_Y(\zeta), H(\zeta), \rho(\zeta)\}$ has been generated with different distribution information by using Sobol's sequence as listed in Table 4. The selected system properties are significant for the impact resistance of structure and an additional 10e3 cycles of MCS simulation is set as the reference result, which can be seen clear in Fig. 8, with grey curves shown all the random impact responses and a blue dashed curve shows the deterministic impact response at point A. From Fig. 8, the red region at the top of figure illustrates the failure region which exceeds the safety threshold, such that the dynamic response in the failure area is marked with 'fail' status for the structure.

To construct the VMASA model, a converged training sample size needs to be determined first for the CXSVR algorithm. Based on the DoE, various training sample size levels have been adopted to train the model and the predicted Z-displacement results are compared with MCS results through measures of R^2 and RMSE, as shown in Fig. 9. From Fig. 9, the accuracy of R^2 increase with the rise of training sample, and at the size of 200, the value is stable with 0.995; the value of RMSE decreases with the rise of training sample and is stable with 0.232 at the same size. The training sample size of the virtual model is determined as $N_{train} = 200$.

The maximum Z-direction displacement and maximum von Mises stress at point A are predicted and compared with MCS results as shown in Figs. 10–11. In Figs. 10–11, the probability density function (PDF), cumulative density function (CDF) and the relative errors for the CDF curves are presented for both displacement and stress responses. It is clear from the results that the virtual modelling technique coincides well with the reference in both curves.

In addition, the detailed statistical moments (i.e., mean and standard deviation) of the maximum deflection and stress from two approaches are provided in Table 5. In Table 5, the moments of the predicted responses are matched well with the reference values, with the absolute maximum relative error of only 1.117%. Consequently, seen from both reliability profiles and statistical moments, the accuracy of the proposed virtual modelling technique has been well illustrated. However, considering the computational efforts, the proposed framework takes only quarter of the efforts used by the conventional MCS method. The detailed computational time for the VMASA method is 33.6 h for training samples' simulation, 0.5 h for the surrogate model construction and 5 s for prediction of varying inputs. The proposed framework is efficient on handling dynamic analysis with various system information.

The probability of failure at point A by two approaches are listed in Table 6. From Table 6, the MCS-derived probability of failure of maximum Z-direction displacement at point A calculated by MCS approach is $p_f = 0.121$. For the VMASA technique, the probability of

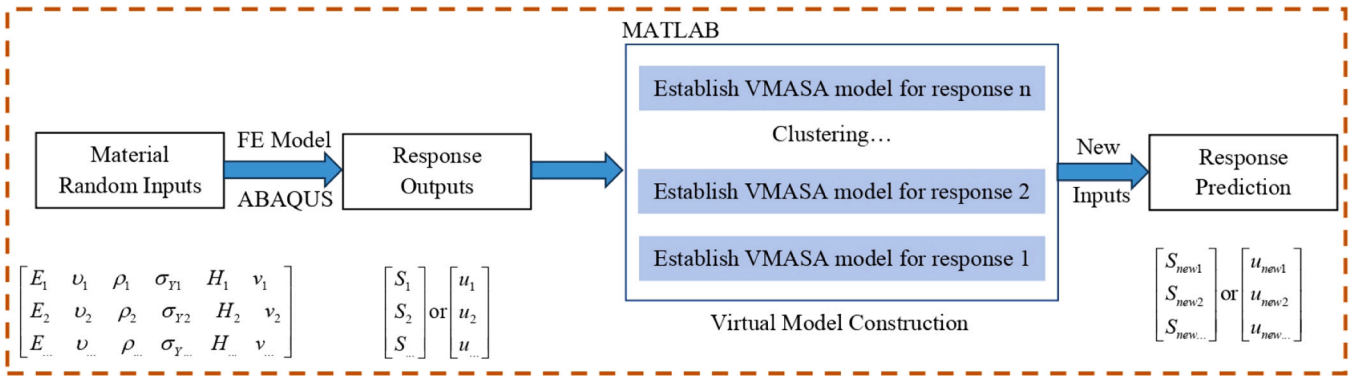

Fig. 13. VMASA virtual model training procedure.

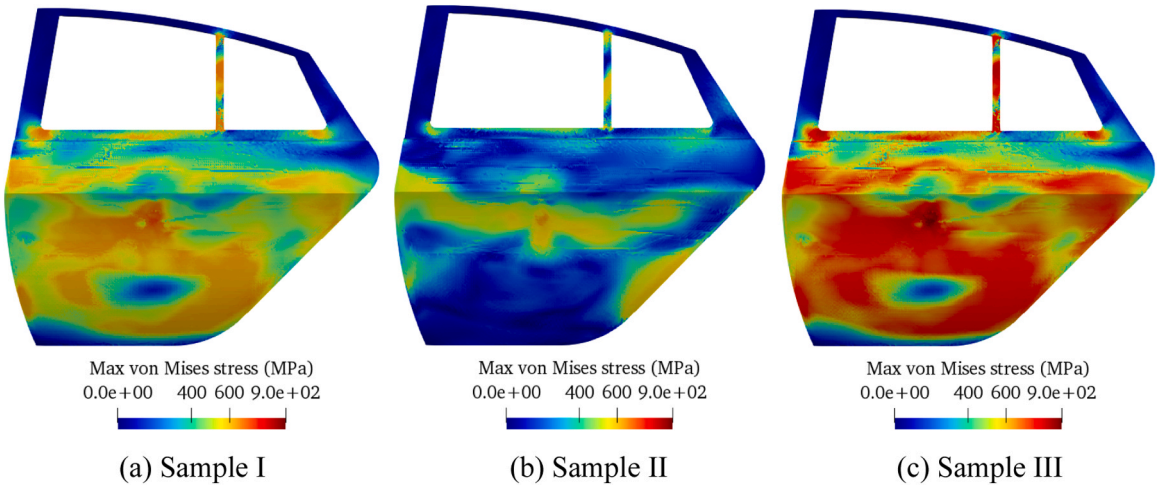

Fig. 14. VMASA predicted von Mises stress distribution of car door at three new sample points.

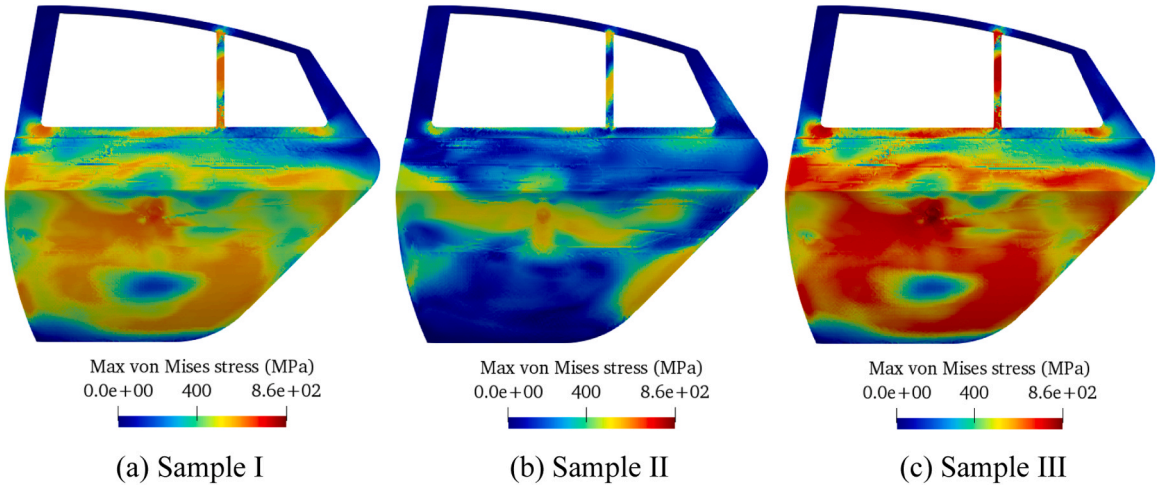

Fig. 15. Numerical von Mises stress distribution of car door at three new sample points.

failure estimated by the CXSVR algorithm gradually converges to the MCS-derived probability with the increase of training sample size. At the size of 200, the predicted probability of failure at point A is $\widehat{p}_f = 0.122$, which is almost identical to the MCS-derived probability of failure, but in an efficient manner.

In Fig. 12, all the predicted responses at the entire sample space from the virtual model have been shown and the corresponding limit state function surface established by the VMASA model has been visibly shown for better understanding. From the limit state function surface, readers can easily see and classify the 'safe' and 'fail' regions for arbitrary training sample, which constructs the critical ability of the dynamic safety analysis by using the virtual modelling.

The dynamic safety analysis framework is competent to predict the 'safe' or 'fail' status of structure towards the forecasted information. In

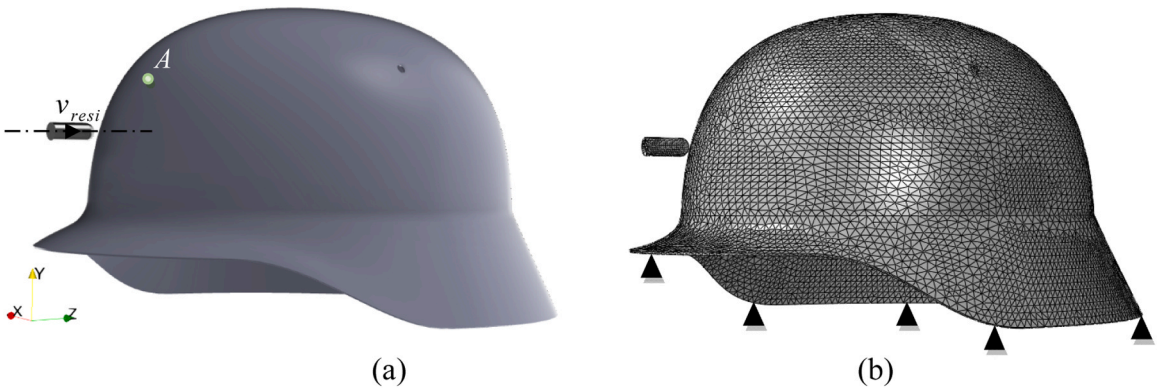

Fig. 16. Numerical example 3: (a) stahlhelm geometry, (b) mesh plot and boundary conditions.

Table 9
Distribution of inputs for stahlhelm.

Varying Inputs	Distribution type	Mean	Standard deviation	Interval
E (GPa)	Normal[28]	190	9.5	-
υ	Lognormal[47]	0.32	0.016	-
ρ (kg/m^3)	Cauchy	7630	381.5	-
σ_Y (GPa)	Weibull	0.31	0.0155	-
H	Uniform	–		[800,900]

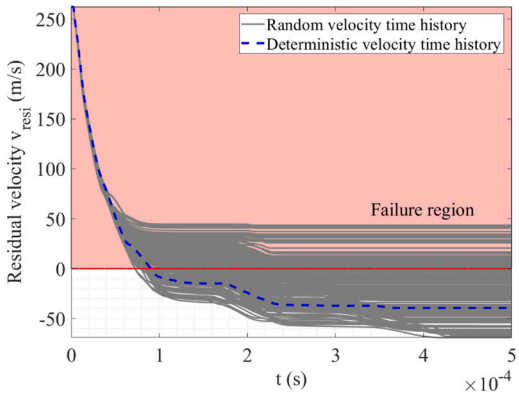

Fig. 17. Random velocity time history and failure region of the bullet impactor.

here, three new arbitrary sample events are generated and implemented into the established surrogate model as listed in Table 7. The estimation results are rigorously verified with the deterministic finite element numerical results at three samples. As listed in Table 8, the safety conditions of three new samples are identified with 'Fail', 'Safe' and 'Fail' by the proposed technique, which are identical with the MCS-derived results. Also, the limit state functions have been estimated by the VMASA algorithm to better classify the structural safety. After validating the accuracy, the total prediction time by using the virtual model is only 5 s and saved 99% computational time of the deterministic finite element analysis. This capability provides accurate and efficient safety assessment for engineering structures under dynamic excitations.

Furthermore, due to the clustering virtual modelling capabilities of the proposed technique as shown in Fig. 13, the overall von Mises stresses in the structural body can be predicted as presented in Figs. 14–15. The deterministic numerical results are also provided to illustrate the accuracy of the VMASA model. It can be seen that the estimated structural stress conditions simulate well with the deterministic responses at all three samples. The relative errors between three samples are less than 5%, which are accurate enough for practical engineering applications to visibly observe the entire structural stress distribution and make forecast before certain stress concentration happens.

4.3. Stahlhelm

For the third numerical case, a practical stahlhelm is impacted by a high-velocity bullet, with the impact velocity of 262 m/s. The radius of the helmet is about 15 cm with thickness of 0.5 cm, and the diameter of the impactor is 0.6 cm. The stahlhelm is made of steel material and a

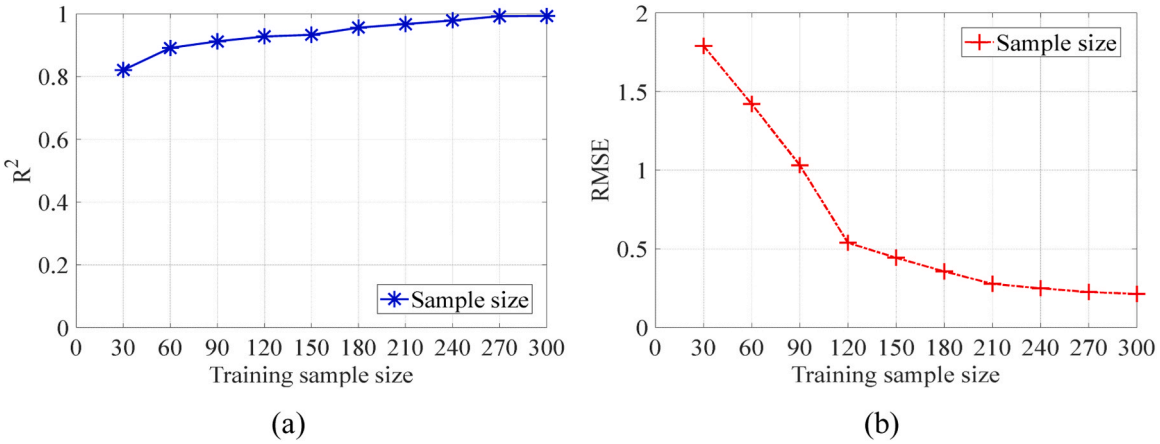

Fig. 18. The estimated (a) R^2 and (b) *RMSE* of Z-disp with different training sample size.

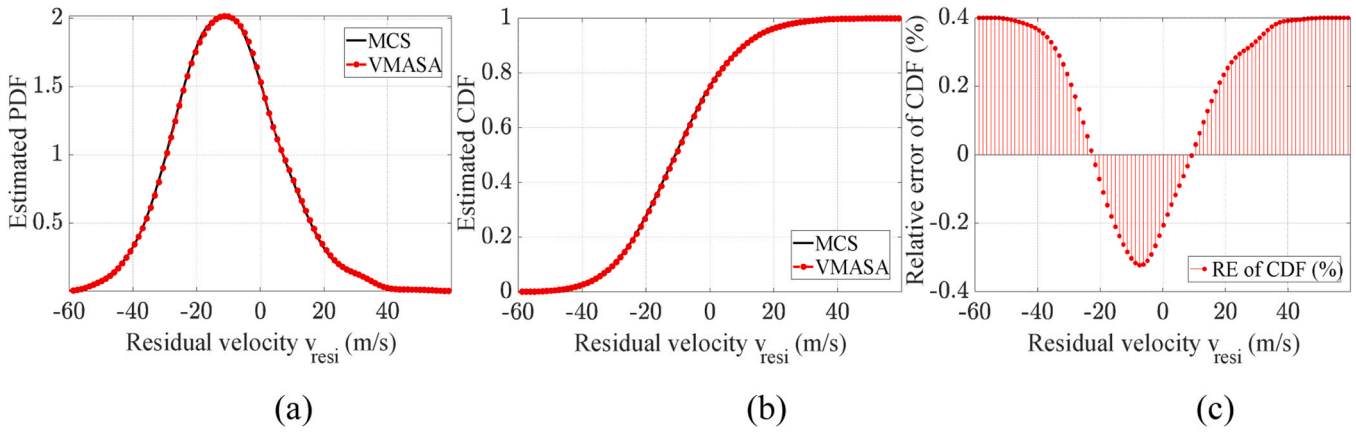

Fig. 19. (a) The estimated PDFs; (b) CDFs; (c) *RE* of CDFs of residual velocity v_{resi}.

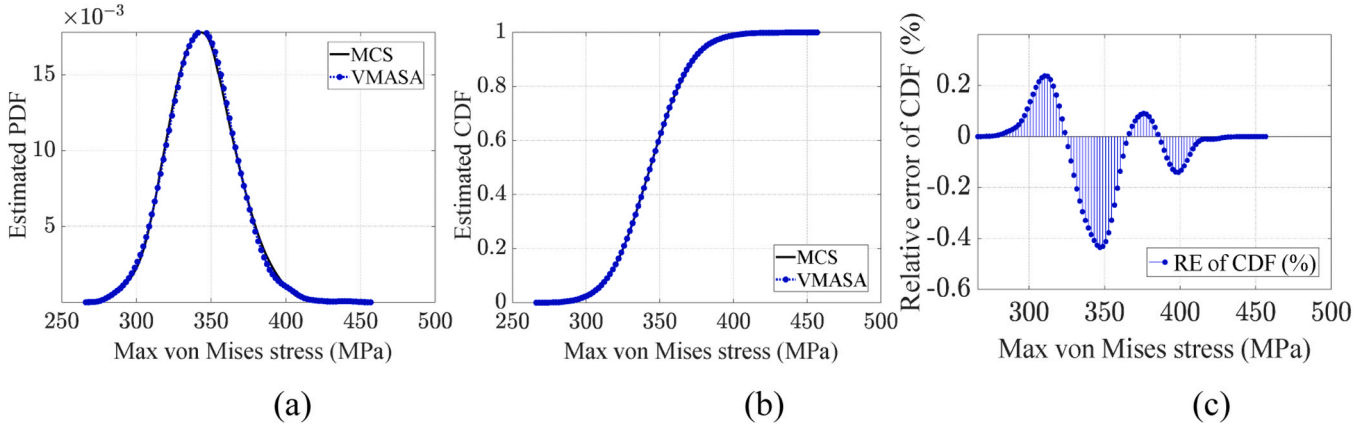

Fig. 20. (a) The estimated PDFs; (b) CDFs; (c) *RE* of CDFs of maximum von Mises stress.

Table 10
The estimated moments of residual velocity and von Mises stress.

Moments	Methods	v_{resi} (m/s)	*RE* (%)	Max vM stress (MPa)	*RE* (%)	Computational cost (h)
Mean	VMASA	-12.624	-0.008	344.130	0.0552	76.9
	MCS	-12.521	–	343.940	–	254.2
Std	VMASA	0.195	-0.510	21.966	0.164	76.9
	MCS	0.196	–	21.930	–	254.2

Table 11
The probability of failure of residual velocity of bullet exceeds $|\delta|$.

Methods	$\widehat{p}_f$ (N_{train}=60)	RE_{p_f} (%)	$\widehat{p}_f$ (N_{train}=150)	RE_{p_f} (%)	$\widehat{p}_f$ (N_{train}=300)	RE_{p_f} (%)
VMASA	0.009	-72.727	0.025	-24.242	0.043	0
MCS	p_f = 0.043					

strain hardening effect has been considered for the stahlhelm. The geometry of the stahlhelm and impactor are shown in Fig. 16(a), by using the tetrahedron finite element, a converged mesh of geometry is shown in Fig. 16(b). For the boundary conditions of the stahlhelm application, the nodes on the bottom external edges of the sthlhelm are fixed in all directions which have been highlighted in Fig. 16(b) through black triangular symbols and the z-direction impact loading was applied at the central location of the helmet surface.

The structure is considered safe only if the single-time bullet didn't penetrate the helmet. That is, the residual velocity v_{resi} of the bullet is less than 0, which means the bullet would bounce back after contacting, otherwise if $v_{resi} > 0$, the bullet would penetrate through the helmet and make damage to human head. Thus, for this case, a residual velocity based first-passage theory should be adopted. For instance, the residual velocity of the bullet is selected as the observation response and the safety threshold of bullet is set to be $|\delta| = 0\text{m/s}$. Also, the maximum von Mises stress at point A is observed to monitor the stress distribution of helmet. The residual velocity-based limit state function in this example is represented as

$$g(\boldsymbol{\xi}, t) = v_{resi}(\boldsymbol{\xi}, t) - |\delta| = v_{resi}(\boldsymbol{\xi}, t) - 0 \tag{26}$$

where the limit state function $g < 0$, the structure is safe, otherwise

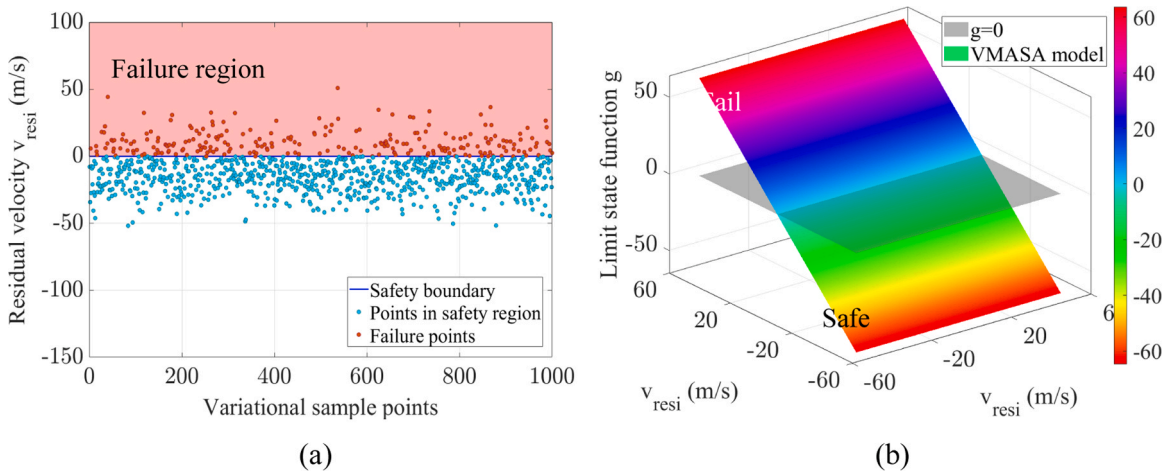

Fig. 21. (a) The estimated residual velocity and (b) limit state function at different input samples through the VMASA model.

Table 12
Three arbitrary groups of new input samples.

Varying Inputs	Sample I	Sample II	Sample III
E (GPa)	164.5	191.4	236.9
υ	0.3043	0.3653	0.3410
ρ (kg/m^3)	7122	7762	7699
σ_Y (GPa)	0.291	0.312	0.326
H	882.1	826.2	802.1

Table 13
The predicted safety status of stahlhelm with three arbitrary new samples.

Samples	Methods	v_{resi} (m/s)	RE (%)	Safety status	Computational cost (min)
I	VMASA	-16.96	5.725	Safe, g= −16.96	0.11
	Numerical	-17.99	–	Safe, g= −17.99	15.3
II	VMASA	8.31	3.616	Fail, g= 8.31	0.11
	Numerical	8.02	–	Fail, g= 8.02	15.3
III	VMASA	-3.51	-5.089	Safe, g= −3.51	0.11
	Numerical	-3.34	–	Safe, g= −3.34	15.3

failed.

For the varying input samples, the random vector $\boldsymbol{\xi} = \{E(\zeta), \upsilon(\zeta), \sigma_Y(\zeta), H(\zeta), \rho(\zeta)\}$ has been generated with different distribution information by using Sobol's sequence as listed in Table 9. The selected system properties are significant for the impact resistance of structure and an additional 10e3 cycles of MCS simulation is set as the reference result, which can be seen clearly in Fig. 17, with grey curves shown all the random velocity time histories and a blue dashed curve shows the deterministic velocity time history of the bullet. From Fig. 17, the red region at the top of figure illustrates the failure region which exceeds the safety threshold, such that the dynamic response in the failure area is marked with 'fail' status for the structure.

To construct the VMASA model, a converged training sample size needs to be determined first for the CXSVR algorithm. Based on the DoE, various training sample size levels have been adopted to train the model and the predicted results are compared with MCS results through measures of R^2 and RMSE, as shown in Fig. 18. From Fig. 18, the accuracy of R^2 increase with the rise of training sample, and at the size of 300, the value is stable with 0.998; the value of RMSE decreases with the rise of training sample and is stable with 0.192 at the same size. Therefore, the ultimate sample size of the virtual model is determined as $N_{train} = 300$.

The residual velocity of bullet and maximum von Mises stress at point A are predicted and compared with MCS results as shown in Figs. 19–20. In Figs. 19–20, the PDF, CDF and the relative errors for the CDF curves are presented for both velocity and stress responses. Based on the results, it is clear the results from the VMASA technique coincides well with the reference results in both PDF and CDF curves.

In addition, the detailed statistical moments of the residual velocity and stress from two approaches are provided in Table 10. In Table 10, the moments of the predicted responses are matched well with the reference values, with the absolute maximum relative error of only 0.510%. However, considering the computational efforts, the proposed framework takes only quarter of the efforts used by the conventional MCS method. The detailed computational time for the VMASA method is 76.3 h for training samples' simulation, 0.6 h for the virtual modelling model construction and 7 s for the prediction of varying inputs.

Furthermore, the probability of failure of bullet by two approaches are listed in Table 11. From Table 11, the MCS-derived probability of failure of residual velocity of bullet calculated by MCS approach is $p_f =$

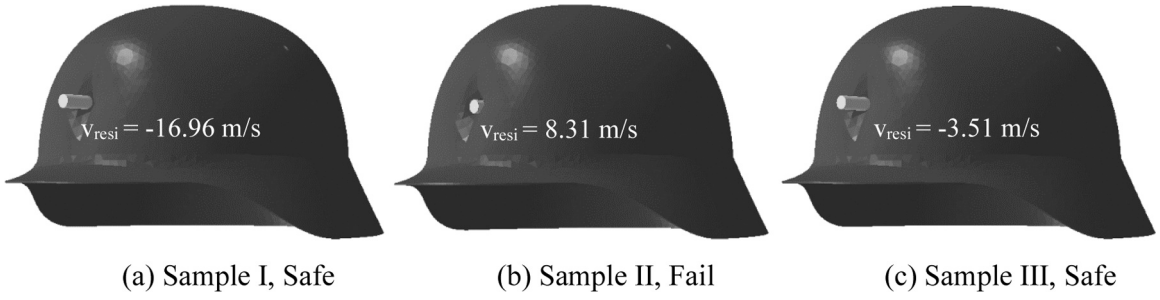

Fig. 22. VMASA predicted residual velocity of bullet for three new sample points.

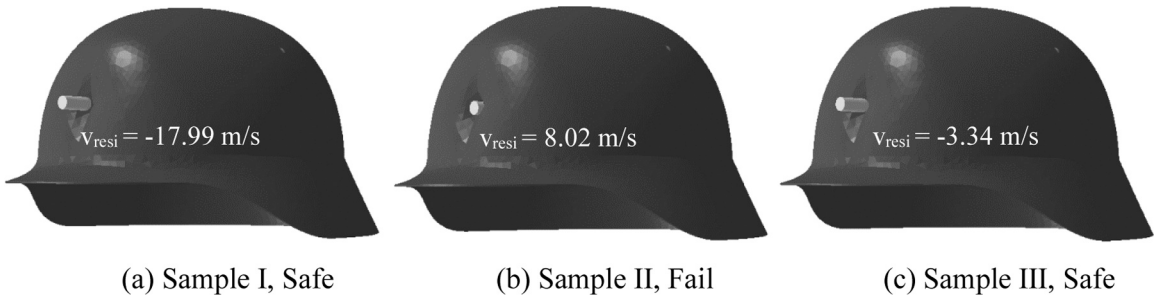

Fig. 23. Numerically calculated residual velocity of bullet for three new sample points.

0.043. For the virtual modelling technique, the probability of failure estimated by the CXSVR algorithm gradually converges to the MCS-derived probability with the increase of training sample size (i.e., 60, 150, 300). At the size of 300, the predicted probability of failure is $\widehat{p}_f = 0.043$, which is just identical to the MCS-derived probability of failure. In Fig. 21, all the predicted responses at the entire sample space from the VMASA model have been shown and the corresponding limit state function surface established by the VMASA model has been visibly shown for better understanding. From the limit state function surface, readers can easily review and classify the 'safe' and 'fail' regions for arbitrary training sample.

Once again, the proposed dynamic safety assessment framework is capable of predicting the 'safe' or 'fail' status of structure against future forecasted information. Here, three new arbitrary sample events are generated in Table 12 then implemented into the established virtual modelling model. The estimation results are rigorously verified with the deterministic finite element numerical results at three samples. As listed in Table 13, the safety conditions of three new samples are identified with 'Safe', 'Fail' and 'Safe' by the proposed technique, which are identical with the MCS-derived results. Also, the limit state functions have been estimated by the VMASA algorithm to better classify the structural safety. After validating the accuracy, the total prediction time by using the VMASA model is only 7 s and saved 99% computational time of the deterministic finite element analysis. This capability provides both accurate and efficient safety assessment for the critical structures under dynamic excitations.

Furthermore, the schematics of residual velocities of bullet can be virtually predicted following in procedure in Fig. 13 and the results are presented in Figs. 22–23. The deterministic numerical results are also provided to illustrate the accuracy of the VMASA model. It can be seen that the estimated residual velocity of bullet matches well with the deterministic velocity for all three new samples. The relative errors between the three samples are not larger than 10%, which are acceptable for practical engineering applications to visibly observe the high velocity impact process and make forecast against the future changing system information.

5. Conclusion

In this paper, a sampling-based dynamic safety assessment framework by using the virtual modelling technique (VMASA) was proposed for ductile materials against high-velocity impact loadings. The reliability analysis was adopted through the first-passage theory and a popular Johnson Cook model was used to simulate the plastic deformation of ductile material under high-velocity impact. For the virtual modelling technique, a new machine learning algorithm, namely the clustering extended support vector regression (CXSVR) was implemented to analyse the inherent relationship between the varying inputs and structural dynamic plastic deformations caused by impact loadings. A new T-spline kernel was developed to enhance the performance of the machine learning algorithm especially for the complex engineering problems. Based on the explicit regression functions obtained by the virtual model, the proposed safety analysis framework was competent to predict the potential structural response and assess the safe or fail condition of the structure against the continuously varying system information, which was called the forecasting capability for practical applications. Through the VMASA model, the repetitive FEM analysis by using the conventional Monte Carlo simulation method has been eliminated such that a great deal of computational efforts can be saved. By calculating several practical experimental and numerical investigations, the accuracy, efficiency, and practicability of the proposed safety assessment framework were demonstrated under various conditions.

Furthermore, the proposed strategy has been shown with potentials for further structural design and optimization fields. Research investigations about the advanced composite structures' performance under impact loadings, and the next-step material/topology optimization will be conducted in future research works.

CRediT authorship contribution statement

Yuan Feng: Conceptualization, Software, Methodology, Writing – original draft. **Mehrisadat Makki Alamdari:** Software, Writing, Methodology. **Di Wu:** Software, Methodology. **Zhen Luo:** Software, Methodology. **Dong Ruan:** Writing – original draft, Writing – review & editing, Supervision, Methodology. **Temitope Egbelakin:** Software, Writing – review & editing. **Xiaojun Chen:** Software, Writing – review & editing. **Wei Gao:** Writing – review & editing, Supervision, Methodology.

Declaration of Competing Interest

The authors declare that they have no known competing financial interests or personal relationships that could have appeared to influence the work reported in this paper.

Data availability

No data was used for the research described in the article.

Acknowledgements

The work presented in this paper is supported by the Australian Research Council projects IH200100010, DP210101353, DP230102781, DP240102559 and IH210100048, and the China Scholarship Council (No. 201706120056). The research work has been undertaken with the assistance of resources and services from the National Computational Infrastructure (NCI) Australia.

Appendix A. Definitions of optimization parameters

The vectors and matrices of $\mathbf{Q}_k$ and $\mathbf{m}_k$ defined in the CXSVR optimization algorithm are expressed as:

$$\mathbf{Q}_k \in \Re^{4m\times 4m} := \left(\widehat{\mathbf{R}}_k + \mathbf{I}_{4m\times 4m}\right)\widehat{\mathbf{T}}_k^{-1}\left(\widehat{\mathbf{R}}_k + \mathbf{I}_{4m\times 4m}\right)^T + \widehat{\mathbf{H}}_k\widehat{\mathbf{e}}_k\widehat{\mathbf{e}}_k^T\widehat{\mathbf{H}}_k \tag{A1}$$

$$\mathbf{m}_k \in \Re^{4m} := \lambda_2\left(\widehat{\mathbf{R}}_k + \mathbf{I}_{4m\times 4m}\right)\widehat{\mathbf{T}}_k^{-1}\mathbf{u}_k - \varepsilon\widehat{\mathbf{e}}_k - \widehat{\mathbf{k}}_k \tag{A2}$$

$$\widehat{\mathbf{T}}_k = \begin{bmatrix} \lambda_1\mathbf{I}_{m\times m} & & & \\ & \lambda_1\mathbf{I}_{m\times m} & & \\ & & S\mathbf{I}_{m\times m} & \\ & & & S\mathbf{I}_{m\times m} \end{bmatrix} \tag{A3}$$

$$\widehat{\mathbf{H}}_k = \begin{bmatrix} \mathbf{0}_{2m\times 2j} & \mathbf{0}_{2m\times m} & \mathbf{0}_{2m\times m} \\ \mathbf{0}_{m\times 2m} & \mathbf{I}_{m\times m} & \mathbf{0}_{m\times m} \\ \mathbf{0}_{m\times 2m} & \mathbf{0}_{m\times m} & -\mathbf{I}_{m\times m} \end{bmatrix} \tag{A4}$$

$$\widehat{\mathbf{R}}_k = \begin{bmatrix} \mathbf{0}_{2m\times m} & \mathbf{0}_{2m\times m} & \mathbf{0}_{2m\times 2m} \\ -\boldsymbol{\xi}_{train} & \boldsymbol{\xi}_{train} & \mathbf{0}_{m\times 2m} \\ \boldsymbol{\xi}_{train} & -\boldsymbol{\xi}_{train} & \mathbf{0}_{m\times 2m} \end{bmatrix} \tag{A5}$$

$$\mathbf{u}_k = \begin{bmatrix} \mathbf{e}_m \\ \mathbf{e}_m \\ \mathbf{0}_{2m} \end{bmatrix}, \quad \widehat{\mathbf{e}}_k = \begin{bmatrix} \mathbf{0}_{2m} \\ \mathbf{e}_m \\ \mathbf{e}_m \end{bmatrix}, \quad \widehat{\mathbf{k}}_k = \begin{bmatrix} \mathbf{0}_{2m} \\ \mathbf{y}_{train} \\ -\mathbf{y}_{train} \end{bmatrix}, \quad \mathbf{v}_k = \begin{bmatrix} \mathbf{p}_k \\ \mathbf{q}_k \\ \vartheta \\ \widehat{\vartheta} \end{bmatrix} \tag{A6}$$

References

[1] Tinoco MP, Silva FA, Khoddami Maraghi Z. Repair of pre-damaged RC beams using hybrid fiber reinforced strain hardening cementitious composites. Eng Struct 2021;235:112081.
[2] Ryu J, Lee CH, Park MJ, Ju YK. Experimental study on bearing behavior of glass fiber steel composite plates (GSPs) for bolted connections. Eng Struct 2019;186:170–82.
[3] Fras T, Pawlowski P, Li W, Wierzbicki T. Performance of Li-ion pouch batteryunder a high-velocity impact: experiment and numerical simulation. Int J Impact Eng 2021;155:103915.
[4] Guo X, Zhang C, Chen ZQ. Experimental and numerical assessment of scoured bridges with protective bonded steel plates against vessel impact. Eng Struct 2022;252:113628.
[5] Feng Y, Wang QH, Yu YG, Zhang TY, Wu D, Chen XJ, Luo Z, Gao W. Experimental-numerical-virtual (ENV) modelling technique for composite structure against low velocity impacts. Eng Struct 2023;278:115488.
[6] Huang S, Qiao P. Nonlinear stability analysis of thin-walled I-section laminated composite curved beams with elastic end restraints. Eng Struct 2021;226:111336.
[7] Signetti S, Heine A. Transition regime between high-velocity and hypervelocity impact in metals – A review of the relevant phenomena for material modeling in ballistic impact studies. Int J Impact Eng 2022:104213.
[8] Jiang C, Huang XP, Han X, Zhang DQ. A time-variant reliability analysis method based on stochastic process discretization. J Mech Des Trans ASME 2014;136:091009.
[9] Chen JB, Li J. The extreme value distribution and dynamic reliability analysis of nonlinear structures with uncertain parameters. Struct Saf 2007;29:77–93.
[10] Jiang C, Ni BY, Han X, Tao YR. Non-probabilistic convex model process: A new method of time-variant uncertainty analysis and its application to structural dynamic reliability problems. Comput Methods Appl Mech Eng 2014;268:656–76.
[11] Montesinos-López OA, Montesinos-López JC, Singh P, Lozano-Ramirez N, Barrón-López A, Montesinos-López A, et al. A multivariate poisson deep learning model for genomic prediction of count data. G3 Genes, Genomes, Genet 2020;10:4177–90.
[12] Coleman JJ. Reliability of aircraft structures in resisting chance failure. Oper Res 1959;7(5):639–45.
[13] Mason AB, Iwan WD. An approach to the first-passage time in random vibration. ASME J Appl Mech 1983;50(3):641–6.
[14] Ren H, Ye Z, Li Z. Anomaly detection based on a dynamic Markov model. Inf Sci (Ny) 2017;411:52–65.
[15] Andrieu-Renaud C, Sudret B, Lemaire M. The PHI2 method: A way to compute time-variant reliability. Reliab Eng Syst Saf 2004;vol. 84:75–86.
[16] Reid B.A.T. Elements of the Theory of Markov Processes and their Applications. Courier Corporation, New York 1997.
[17] Roberts JB. First-passage probabilities for randomly excited systems: Diffusion methods. Probab Eng Mech 1986;1(2):66–81.
[18] Zhu WQ, Deng ML, Huang ZL. First-passage failure of quasi-integrable Hamiltonian systems. ASME J Appl Mech 2002;69(3):274–82.
[19] Schuëller GI, Pradlwarter HJ, Koutsourelakis PS. A critical appraisal of reliability estimation procedures for high dimensions. Probabilistic Eng Mech 2004;19:463–74.
[20] Au SK, Beck JL. Estimation of small failure probabilities in high dimensions by subset simulation. Probabilistic Eng Mech 2001;16:263–77.
[21] Lu C, Feng YW, Liem RP, Fei CW. Improved Kriging with extremum response surface method for structural dynamic reliability and sensitivity analyses. Aerosp Sci Technol 2018;76:164–75.
[22] Wang Z, Wang P. A nested extreme response surface approach for time-dependent reliability-based design optimization. J Mech Des Trans ASME 2012;134:121007.
[23] Yu Y, Gao W, Castel A, Liu A, Feng Y, Chen X, Mukherjee A. Modelling steel corrosion under concrete non-uniformity and structural defects. Cem Concr Res 2020;135:106109.
[24] Hohenbichler M, Gollwitzer S, Kruse W, Rackwitz R. New light on first- and second-order reliability methods. Struct Saf 1987;4:267–84.
[25] Du X. Time-dependent mechanism reliability analysis with envelope functions and first-order approximation. J Mech Des Trans ASME 2014;136:081010.
[26] Silver D, Huang A, Maddison CJ, Guez A, Sifre L, Van Den Driessche G, et al. Mastering the game of Go with deep neural networks and tree search. Nature 2016;529:484–9.
[27] Feng Y, Wang Q, Wu D, Luo Z, Chen X, Zhang T, Gao W. Machine learning aided phase field method for fracture mechanics. Int J Eng Sci 2021;169:103587.
[28] Feng Y, Wang Q, Wu D, Chen X, Gao W. Dynamic virtual modelling technique for structures with geometric-material hybrid nonlinearities. Struct Saf 2023;100(2):102284.
[29] Colasante G, Gosling PD. Including Shear in a Neural Network Constitutive Model for Architectural Textiles. Procedia Eng, vol. 155. Elsevier Ltd,; 2016. p. 103–12.
[30] Rizzo F, Caracoglia L. Examination of artificial neural networks to predict wind-induced displacements of cable net roofs. Eng Struct 2021;245:112956.
[31] Li J, Chen J, Sun W, Peng Y. Advances of the probability density evolution method for nonlinear stochastic systems. Probabilistic Eng Mech 2012;vol. 28:132–42.
[32] Erice B, Pérez-Martín MJ, Gálvez F. An experimental and numerical study of ductile failure under quasi-static and impact loadings of Inconel 718 nickel-base superalloy. Int J Impact Eng 2014;69:11–24.
[33] Islam MRI, Chakraborty S, Shaw A, Reid S. A computational model for failure of ductile material under impact. Int J Impact Eng 2017;108:334–47.
[34] Johnson GR, Cook WH. Fracture characteristics of three metals subjected to various strains, strain rates, temperatures and pressures. Eng Fract Mech 1985;21:31–48.
[35] Banerjee A, Dhar S, Acharyya S, Datta D, Nayak N. Determination of Johnson cook material and failure model constants and numerical modelling of Charpy impact test of armour steel. Mater Sci Eng A 2015;640:200–9.
[36] Murugesan M, Lee S, Kim D, Kang YH, Kim N. A comparative study of ductile damage models approaches for joint strength prediction in hot shear joining process. Procedia Eng, vol. 207. Elsevier Ltd,; 2017. p. 1689–94.
[37] Nossent J, Elsen P, Bauwens W. Sobol' sensitivity analysis of a complex environmental model. Environ Model Softw 2011;26:1515–25.
[38] Tran-Ngoc H, Khatir S, Le-Xuan T, De Roeck G, Bui-Tien T, Abdel Wahab M. A novel machine-learning based on the global search techniques using vectorized data for damage detection in structures. Int J Eng Sci 2020;157:103376.
[39] Tian Y, Li Q, Feng Y, Wu D, Chen X, Gao W. Nonlinear dynamic analysis of the functionally graded porous plates with graphene platelet reinforcement under moving mass. Thin-walled Struct 2022;183:110363.

[40] Zhang H, Dai H, Beer M, Wang W. Structural reliability analysis on the basis of small samples: An interval quasi-Monte Carlo method. Mech Syst Signal Process 2013;37:137–51.
[41] de Angelis M, Patelli E, Beer M. Advanced Line Sampling for efficient robust reliability analysis. Struct Saf 2015;52:170–82.
[42] Feng Y, Wu D, Liu L, Gao W, Tin-Loi F. Safety assessment for functionally graded structures with material nonlinearity. Struct Saf 2020;86:101974.
[43] Kougioumtzoglou IA, Spanos PD. Nonlinear MDOF system stochastic response determination via a dimension reduction approach. Comput Struct 2013;126:135–48.
[44] Fiessler B, Neumann HJ, Rackwitz R. Quadratic limit states in structural realibility. ASCE. J Eng Mech Div 1979;105:661–76.
[45] Hsu CW, Lin CJ. A comparison of methods for multiclass support vector machines. IEEE Trans Neural Netw 2002;13:415–25.
[46] Lenth RV. Response-surface methods in R, using RSM. J Stat Softw 2009;32:1–17.
[47] Ramasamy P, Sampathkumar S. Prediction of impact damage tolerance of drop impacted WGFRP composite by artificial neural network using acoustic emission parameters. Compos Part B Eng 2014;60:457–62.
[48] Feng Y, Wang Q, Wu D, Gao W, Tin-Loi F. Stochastic nonlocal damage analysis by a machine learning approach. Comput Methods Appl Mech Eng 2020;372:113371.
[49] Wang Q, Feng Y, Wu D, Yang C, Yu Y, Li G, Beer M, Gao W. Polyphase uncertainty analysis through virtual modelling technique. Mech Syst Signal Process 2022;162:108013.
[50] Hofmann T, Schölkopf B, Smola AJ. Kernel methods in machine learning. Ann Stat 2008;36:1171–220.
[51] Feng Y, Gao W, Wu D, Tin-Loi F. Machine learning aided stochastic elastoplastic analysis. Comput Methods Appl Mech Eng 2019;357:112576.
[52] Schölkopf B, Mika S, Burges CJC, Knirsch P, Müller KR, Rätsch G, et al. Input space versus feature space in kernel-based methods. IEEE Trans Neural Netw 1999;10:1000–17.
[53] Berry SM, Carroll RJ, Ruppert D. Bayesian smoothing and regression splines for measurement error problems. J Am Stat Assoc 2002;97:160–9.
[54] Bozzini M, Lenarduzzi L, Schaback R. Kernel B-splines and interpolation. Numer Algorithms 2006;41:1–16.
[55] Bazilevs Y, Calo VM, Cottrell JA, Evans JA, Hughes TJR, Lipton S, et al. Isogeometric analysis using T-splines. Comput Methods Appl Mech Eng 2010;199:229–63.
[56] Wang Q, Feng Y, Wu D, Li G, Liu Z, Gao W. Polymorphic Uncertainty Quantification for Engineering Structures via a Hyperplane Modelling technique. Comput Methods Appl Mech Eng 2022;398:115250.
[57] Emmerich M, Yang K, Deutz A, Wang H, Fonseca CM. A multicriteria generalization of Bayesian global optimization. Springe Optim Its Appl 2016;107:229–42.
[58] Zhang HB, Hu DY, Ye XB, Chen X, He YH. A simplified Johnson-Cook model of TC4T for aeroengine foreignobject damage prediction. Eng Fract Mech 2022;269:108523.
[59] Ghadianlou A, Abdullah SB. Crashworthiness design of vehicle side door beams under low-speed pole side impacts. Thin-Walled Struct 2013;67:25–33.
[60] NCAC. Development and Validation of a Finite Element Model for the 2010 Toyota Yaris Passenger Sedan (NCAC 2011-T-001). National Crash Analysis Center, George Washington University, Virginia Campus, Ashburn, Virginia, Washington.
[61] Long CR, Chung Kim Yuen S, Nurick G. Analysis of a car door subjected to side pole impact. Lat Am J Solids Struct 2019;16(8):e226.